Antarctic Science 33(1), 52–72 (2021) © Antarctic Science Ltd 2020 doi:10.1017/S0954102020000450

Tectono-metamorphic evolution and significance of shear-zone lithologies in Akebono Rock, Lützow-Holm Complex, East Antarctica

SOTARO BABA [1], TOMOKAZU HOKADA [2,3], ATSUSHI KAMEI [4], IPPEI KITANO [5], YOICHI MOTOYOSHI [2], PRAYATH NANTASIN [6], NUGROHO IMAM SETIAWAN [7] and DAVAA-OCHIR DASHBAATAR [8]

[1] *Department of Science Education, University of the Ryukyus, Okinawa 903-0213, Japan*
[2] *National Institute of Polar Research, Tokyo 190-8518, Japan*
[3] *Department of Polar Science, The Graduate University for Advanced Studies (SOKENDAI), Tokyo 190-8518, Japan*
[4] *Department of Geosciences, Shimane University, Matsue, Shimane 690-8504, Japan*
[5] *Division of Earth Sciences, Faculty of Social and Cultural Studies, Kyushu University, Fukuoka 819-0395, Japan*
[6] *Department of Earth Sciences, Faculty of Science, Kasetsart University, Bangkok 10900, Thailand*
[7] *Geological Engineering Department, Engineering Faculty, Universitas Gadjah Mada, DI Yogyakarta 55281, Indonesia*
[8] *Mongolian University of Science and Technology Ulaanbaatar 14191, Mongolia*
baba@edu.u-ryukyu.ac.jp

Abstract: We describe a major shear zone exposed at Akebono Rock and discuss its deformation and metamorphic history, with a view to providing a better understanding of the geological history of the Lützow-Holm Complex. Three deformation episodes are recognized: D1 produced open folds (F1), boudinage and a regional ductile foliation, whilst the related metamorphic facies is characterized by stable garnet. F1 folding is dominantly preserved in the eastern part of the study area. During D2, an isoclinal to tight asymmetric F2 folds developed mainly in the west part of the region, accompanied by an S2 shear, under biotite facies retrograde metamorphism. The D3 episode involved the formation of the major shear zone, characterized by mylonite and L-tectonite fabrics, which took place at ~610–660°C and 4–5 kbar. Large, sigmoidal garnet core domains have S-shaped inclusion trails, suggesting that syntectonic garnet growth occurred before the formation of the shear zone. Estimated *P-T* conditions suggest that the sigmoidal garnet-bearing amphibolite was recrystallized at a deeper crustal level and was brought to a higher level during the formation of the shear zone. Crustal-scale deformation involving syntectonic recrystallization and shearing of Akebono Rock is a key issue for reconsidering the evolution of the Lützow-Holm Complex.

Received 28 May 2020, accepted 10 August 2020

Keywords: L-tectonite, mylonite, *P-T-d* path, sigmoidal garnet

Introduction

During the assembly of the Gondwana supercontinent, an orogenic belt, stretching for > 8000 km, formed along what is now parts of East Africa, southern India, Sri Lanka and East Antarctica. Its various parts are known as the 'East Africa-Antarctica Orogen' (EAAO; Fig. 1a; Jacobs & Thomas 2004), 'East Africa Orogen' (EAO; Stern 1994) or the younger 'Kuunga Orogen' (Meert 2003). In East Antarctica, the central part of Dronning Maud Land (DML) occupies the junction between the Kuunga Orogen and the EAO. Rocks from several localities in central DML contain zircons (dated using U-Pb methods) that indicate metamorphic events occurred at *c.* 640, 600 and 520 Ma (Baba *et al.* 2015). Baba *et al.* (2015) proposed a preliminary model dividing the central DML terrane into six units, based upon a combination of the protolith age and the timing of metamorphism (Fig. 1b, Terrane boundary B). A similar tectonic framework and evolution for other parts of DML have been proposed recently by Osanai *et al.* (2013) and Jacobs *et al.* (2017). According to these studies, many of the unit boundaries appear to be shear zones. Given the potential importance of such shear zones in the tectonic evolution of the region, we decided to study in detail one such shear zone located at Akebono Rock in the Lützow-Holm Complex (LHC) on Prince Olav Coast.

The LHC is variably exposed along the Prince Olav Coast of East Antarctica (Fig. 1b). It is an amphibolite to granulite-facies metamorphic terrane (Hiroi *et al.* 1991). Although the LHC is located outside of the EAAO, it was affected by the Kuunga Orogeny (550 ± 50 Ma). It has been correlated with the basement rocks of India and Sri Lanka (e.g. Shiraishi *et al.* 1994, Meert 2003). The basement rocks of Cape Hinode and Kasumi Rock on the Prince Olav Coast (Fig. 1c) have protolith ages of 1020–984 Ma (Shiraishi *et al.* 1994, 2003, Tsunogae *et al.* 2015) and metamorphic ages of

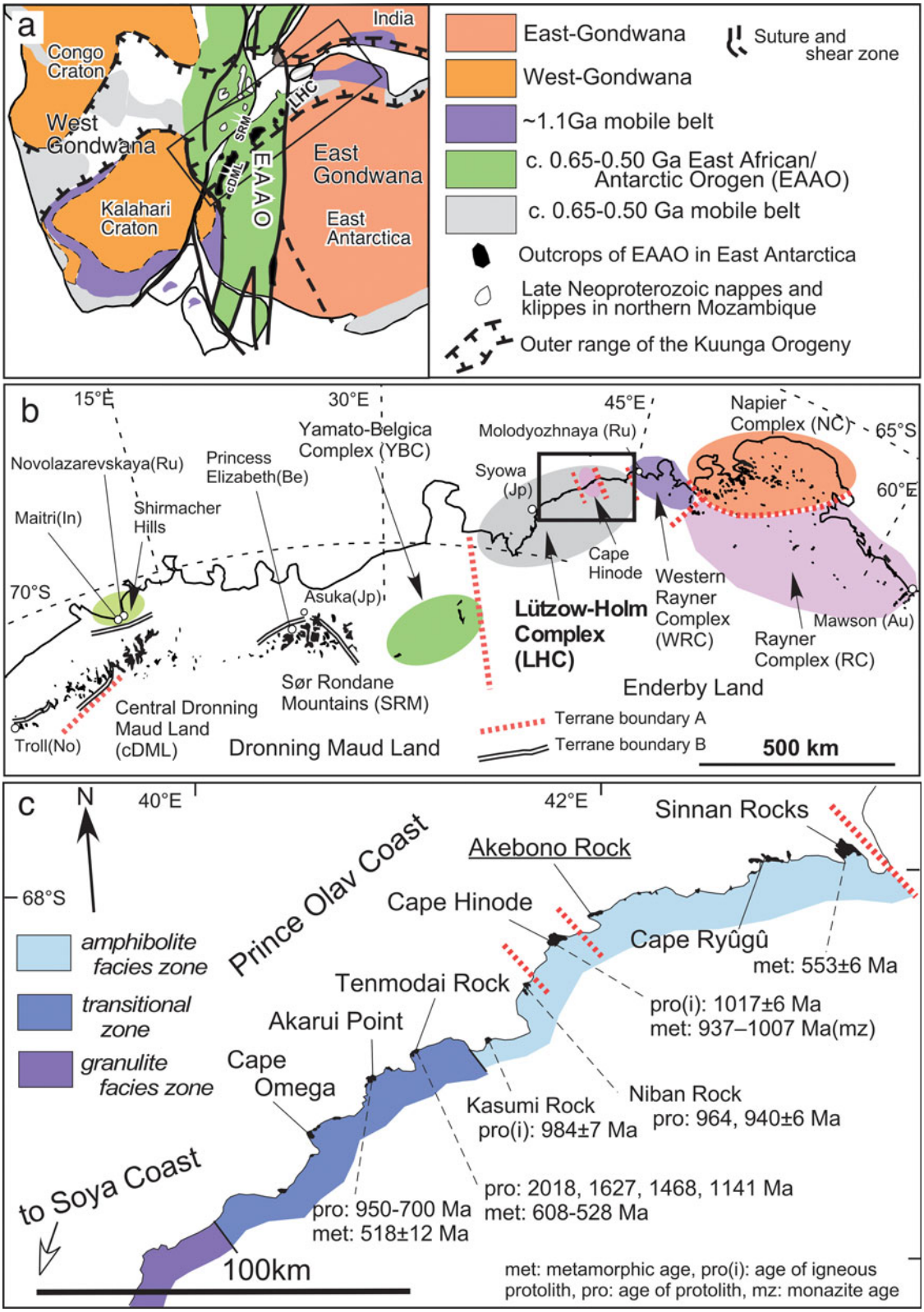

Fig. 1. a. Geological setting of the southern part of the East African-Antarctic Orogen (EAAO), modified after Jacobs & Thomas (2004) and Meert (2003). **b.** Overview map of Dronning Maud Land and Enderby Land, Antarctica. Terrane boundary A is taken from Shiraishi *et al.* (2008) and Jacobs *et al.* (2017). Terrane boundary B is taken from and Osanai *et al.* (2013) and Baba *et al.* (2015). **c.** Location map of Lützow-Holm Complex in the Prince Olav Coast showing metamorphic zones after Hiroi *et al.* (1991). Ages obtained using U-Pb zircon and the monazite chemical isochron method (CHIME) are shown (see text).

https://doi.org/10.1017/S0954102020000450 Published online by Cambridge University Press

1007–935 Ma (Hiroi *et al.* 2008). Thus, in those areas, the characteristic metamorphic age (550 ± 50 Ma) of the LHC has not been detected. At Cape Hinode, the metamorphic grade is granulite-facies, in contrast to the surrounding amphibolite facies of the rest of the Prince Olav Coast (Hiroi *et al.* 2006, 2008). On this basis, Hiroi *et al.* (2006) proposed that Cape Hinode is a Mesoproterozoic allochthonous block that has been tectonically emplaced over the Early Palaeozoic LHC. The timing and mechanism of emplacement of this granulite-facies block are currently unknown, in part because it contacts with the surrounding amphibolite facies terrane are not exposed. Our study of the shear zone exposed at Akebono Rock, which is located close to Cape Hinode (Fig. 1c), has the potential to shed some light on this problem. At Akebono Rock, a shear zone is shown on the regional geological map of Hiroi *et al.* (1986). Such a shear zone close to the obviously allochthonous granulites of Cape Hinode suggests the possibility that it was formed as part of a larger system, which was also responsible for the emplacement of the Cape Hinode granulite block. Here, we report the structural details of the shear zone of Akebono Rock, together with the mineral chemistry and metamorphic conditions of the various lithological units that comprise Akebono Rock. From the results, we derive a set of constraints on models of the evolution of this region. All sample numbers listed in this paper have been simplified from the collection list number of the geology group JARE58 by omitting the prefix 'SB1612'. Mineral abbreviations in the text follow Whitney & Evans (2010), except for quartz, where we prefer to use Qtz.

Geological setting of the LHC

The LHC, which is bounded by the Rayner Complex in the north-east and by the Yamato-Belgica Complex in the south-west (Fig. 1b), consists of high-grade metamorphic rocks and post-metamorphic intrusives. The metamorphic rocks consist of quartzofeldspathic gneisses, intermediate to mafic gneisses, pelitic to psammitic gneisses, charnockites, granitoids, calcsilicates and ultramafics. Previous work (Hiroi *et al.* 1991, Motoyoshi & Ishikawa 1997, Shiraishi *et al.* 1994, Yoshimura *et al.* 2008) has established that there is a general increase in metamorphic grade towards the south-west, reaching ultrahigh-temperature metamorphism in the far south-west, with sensitive high-resolution ion microprobe (SHRIMP) U-Pb zircon ages dating this metamorphic event as occurring 550 ± 50 Ma. These studies also determined that the metamorphic *P-T* paths were clockwise, with peak conditions attributed to kyanite relics. The highest temperature and pressure conditions in the LHC have been estimated to be 950–1040°C and 9–11 kbar at Rundvågshetta (Motoyoshi & Ishikawa 1997).

Recently, SHRIMP U–Pb zircon dating has revealed a more complex metamorphic history, with two events at 645–520 Ma (Takahashi *et al.* 2018, Takamura *et al.* 2018) and 550–520 Ma (Shiraishi *et al.* 1994, 2003), with protolith ages at *c.* 2500, *c.* 1800 and *c.* 1000 Ma (Takamura *et al.* 2018). Based on the detrital zircon ages, lithological assemblages and tectonothermal similarity, Takamura *et al.* (2018) proposed that the LHC on the Soya Coast be divided into three lithological units.

Previous structural studies of several exposures in the LHC have reported multiple deformations, with an early phase of isoclinal folding on which is superimposed a late stage of upright, open folds (Ishikawa *et al.* 1994 and reference therein). Indeed, Ikeda & Kawakami (2004) proposed three phases of deformation at Akarui Point (Fig. 1c). A similar deformation history is reported from the Ongul Islands (Kawakami & Ikeda 2004). Ishikawa *et al.* (1994) concluded that a high-strain, ductile deformation event, which produced a major ductile thrust developed under north-south compression in the northern part of the Rundvågshetta, was followed by a low-strain deformation after peak metamorphism. Based on aerogeophysical data, Nogi *et al.* (2013) proposed a tectonic model involving crustal-scale right-lateral strike-slip movement, resulting in the transposition of the LHC, west Rayner Complex and Rayner Complex.

Field description of Akebono Rock

Akebono Rock (68°05'–68°06'S, 42°54'–43°00') is located near the central part of the Prince Olav Coast, ~12 km north-east from Cape Hinode (Fig. 1c). Hiroi *et al.* (1986) published a 1:25 000 geological map of Akebono Rock (Fig. 2), showing it to be composed principally of metamorphic rocks, including Hbl-Bt gneiss, Bt gneiss, Grt-Bt gneiss, amphibolite, migmatitic leucogranite, granite and pegmatite. Recrystallized mafic dikes intrude into the metamorphic rocks. In this study, we divide the whole exposed area into two parts: east and west regions.

In the east region, compositional banding in metamorphic rock is parallel to a regional foliation, which generally trends NNW-SSE and steeply dips to the east. There is a large, regional-scale, upright antiform that is superimposed on an earlier set of smaller open to closed folds. In this region, there are two types of mafic dikes: an older, well-recrystallized amphibolite (amphibolite II) and slightly metamorphosed basalts and andesites.

In the west region, the general foliation trends towards WNW-ESE and dips steeply to the south. This region is characterized by garnet-bearing leucogranite and pegmatite, amphibolites bearing large garnet porphyroblasts (up to 3 cm) and a major shear zone (Hiroi *et al.* 1986). Generally, this shear zone trends E-W, but turns to run NW-SE at its eastern end of the exposure,

https://doi.org/10.1017/S0954102020000450 Published online by Cambridge University Press

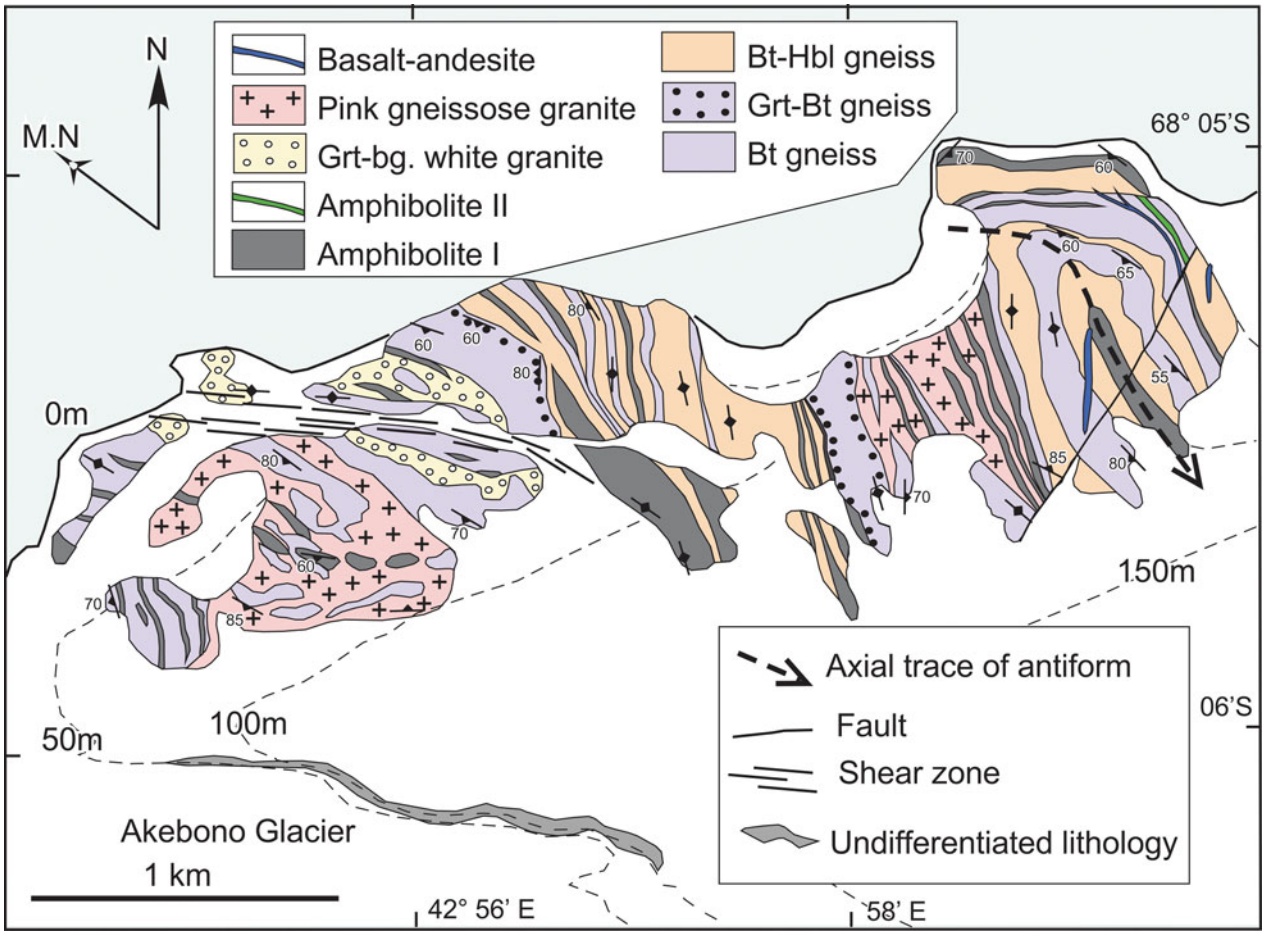

Fig. 2. Geological map of Akebono Rock (modified after Hiroi *et al.* 1986). Grt-bg. = garnet-bearing, Bt-Hbl = biotite-hornblende, Grt-Bt = garnet-biotite, M.N = magnetic north.

where it enters the central region. Mylonitic gneiss and partially deformed Grt-leucogranite are the predominant lithologies exposed adjacent to the shear zone.

Suda *et al.* (2008) report that the mafic metamorphic rocks of Akebono Rock have island-arc affinities. They obtained an Sm-Nd isochron age of 1497 ± 214 Ma and postulated a possible protolith age of *c.* 1500 Ma for the mafic metamorphic rocks at Akebono Rock. However, metamorphic ages from the more reliable U-Pb zircon dating method have yet to be published.

Early deformation of Akebono Rock

The field relationships of basement rocks at Akebono Rock are shown in Figs 3 & 4, while stereo net plots of structures measured in both the east and west regions are shown in Fig. 5. The earliest discernible fabric is a gneissic foliation (S0), defined by compositional banding consisting of intermediate to mafic layers and felsic layers (Fig. 3a). This is especially prominent in the east region.

D1 deformation formed an S1 foliation associated with boudinage (Fig. 3b) and flow folding (F1; Fig. 3c), presumably under ductile conditions. The flow folds, displaying open to tight inter-limb angles, are seen well in coastal exposures in the east region. The leucosome truncates the S0 foliation (Fig. 3a) and presents at the boudin neck. They are folded concordant with the intermediate gneiss (Fig. 3b). There is no significant development of the realignment of mineral grains along the axial planes of F1 folds (Fig. 3c). In addition, there is no consistent discernible orientation of the F1 axial traces at outcrop scale; however, the fold axes mostly plunge at moderate angles to the south. We observe that some folds contain concentrations of garnet, which is not replaced by any secondary minerals, in both their limbs and hinges (Fig. 3d). At a regional scale, we have identified an S1 foliation formed by flattened biotite and hornblende, although in most outcrops it is, for the most part, parallel to S0. Although field measurements show an appreciable scatter in the orientation of the F1 axial planes and the plunge of the fold axes (Fig. 5b), the same stereo net projection shows that the poles to S1 foliations lie very roughly on a great circle, indicating a general plunge of the F1 fold axes at 40°S.

https://doi.org/10.1017/S0954102020000450 Published online by Cambridge University Press

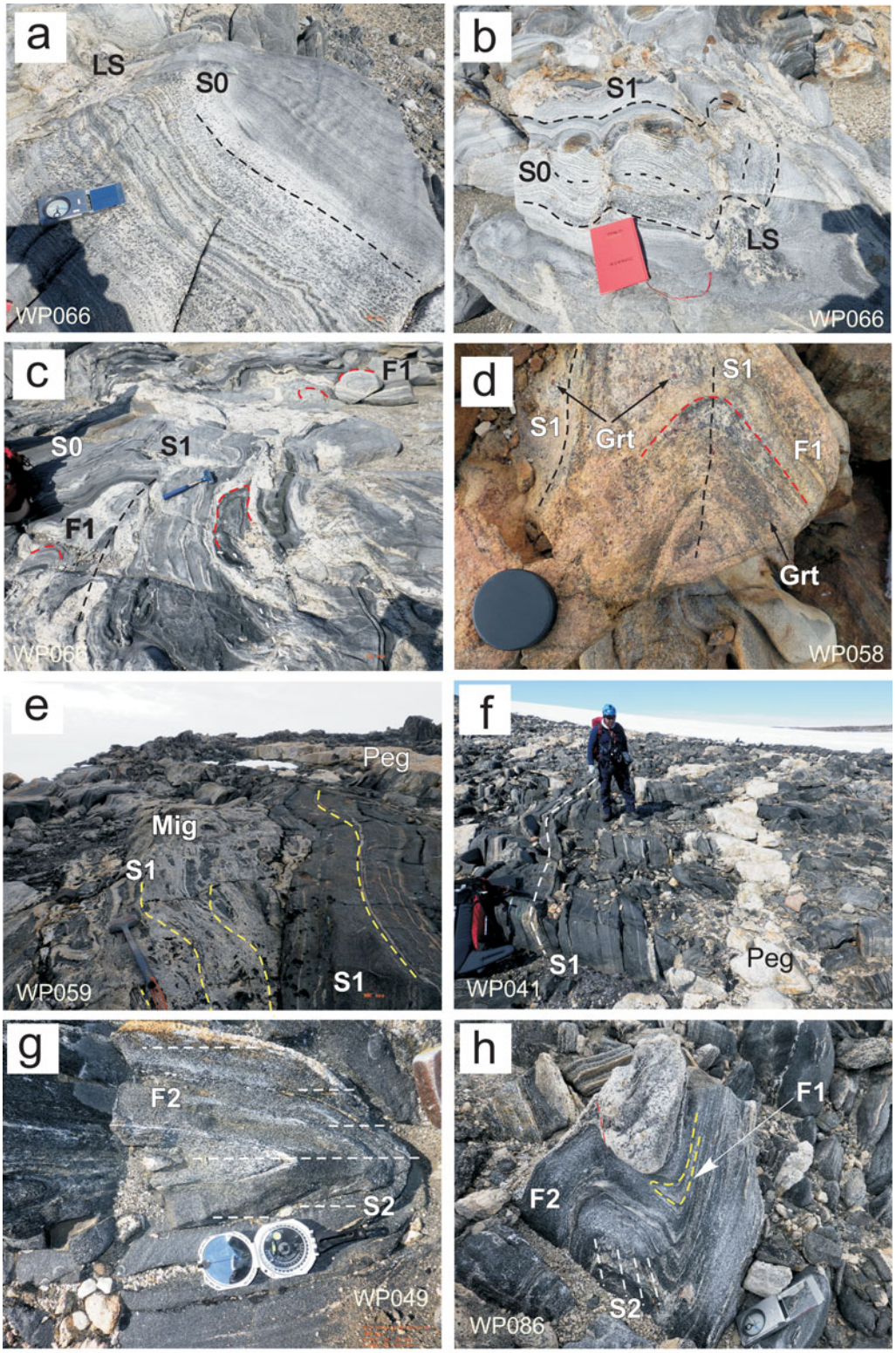

Fig. 3. Photographs of geological structures at Akebono Rock. **a.–c.** Akebono east region. **a.** Compositional banding forms primary foliation S0, here parallel to S1. **b.** Boudinage of coarse compositional banding (S0) and sympathetic deformation of S1. **c.** Flow folds with open to tight style (F1). **d.** Open F1 fold in the west region. Garnets show no replacement by secondary minerals. **e.** Leucocratic migmatite (Mig) containing enclaves of amphibolite and intermediate gneisses with S0/S1 foliation. **f.** Pegmatite (Peg) intruded into amphibolite. **g.** Very tight fold (F2) with weakly developed axial plainer foliation. **h.** Asymmetric F2 fold refolding a rootless F1 fold.

https://doi.org/10.1017/S0954102020000450 Published online by Cambridge University Press

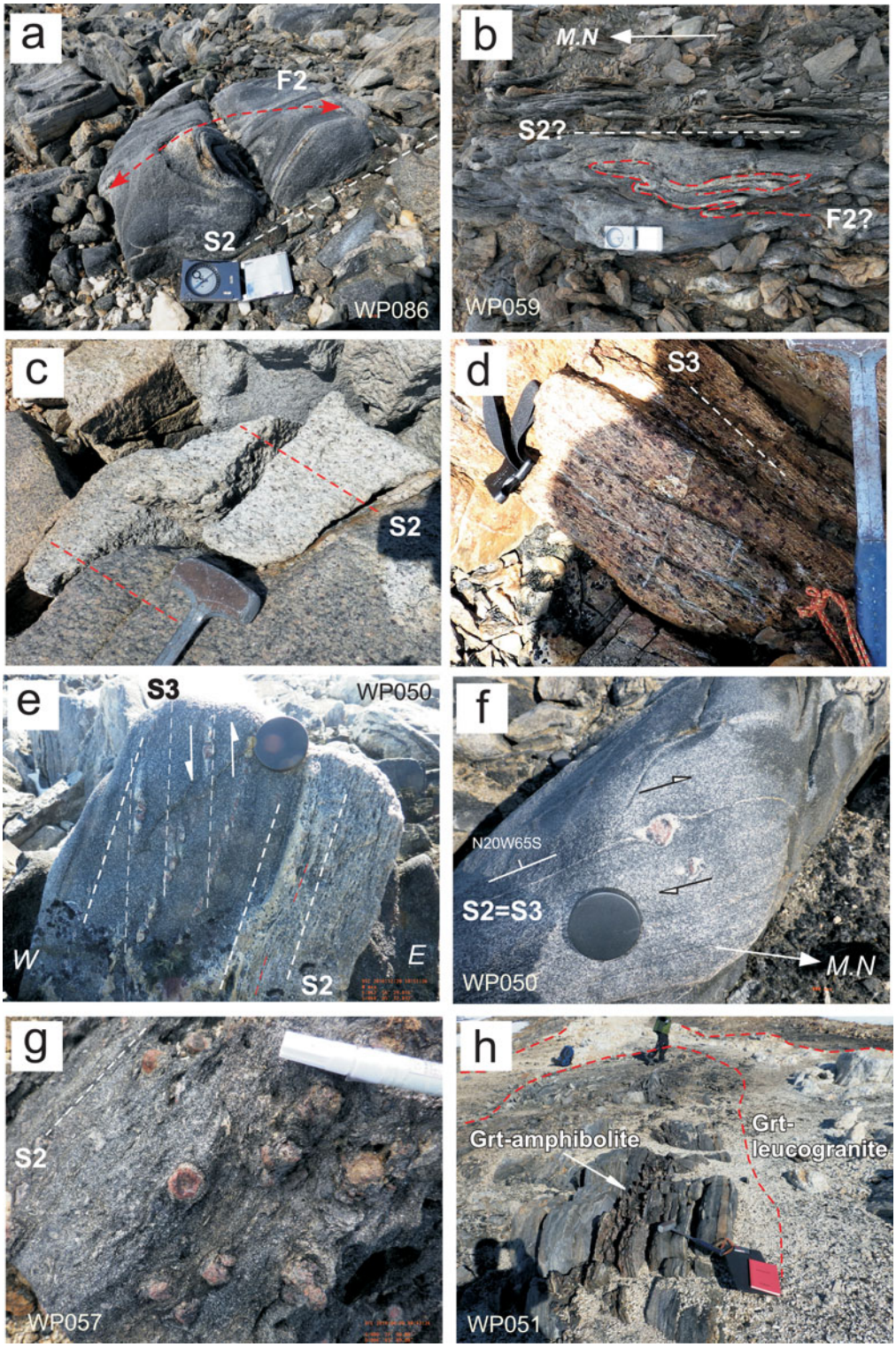

Fig. 4. Photographs of geological structures in the west region of Akebono Rock. **a.** Doubly plunging D2 fold. **b.** Rootless, possible D2 fold within the intensely deformed biotite gneiss. **c.** Garnet partially replaced by biotite, which forms S2 foliation in the garnet-bearing leucogranite. **d.** Mylonite along the D3 shear zone. **e.** Low-strain zone within the D3 shear zone, showing relationship between S2 and S3. **f.** Upper horizontal surface of **e.** showing asymmetric shear indicators developed around large garnets indicating right-lateral shear motion. **g.** Large euhedral to subhedral garnets in amphibolites. **h.** A sigmoidal garnet-bearing amphibolite is enclosed by garnet-bearing leucogranite. M.N = magnetic north.

https://doi.org/10.1017/S0954102020000450 Published online by Cambridge University Press

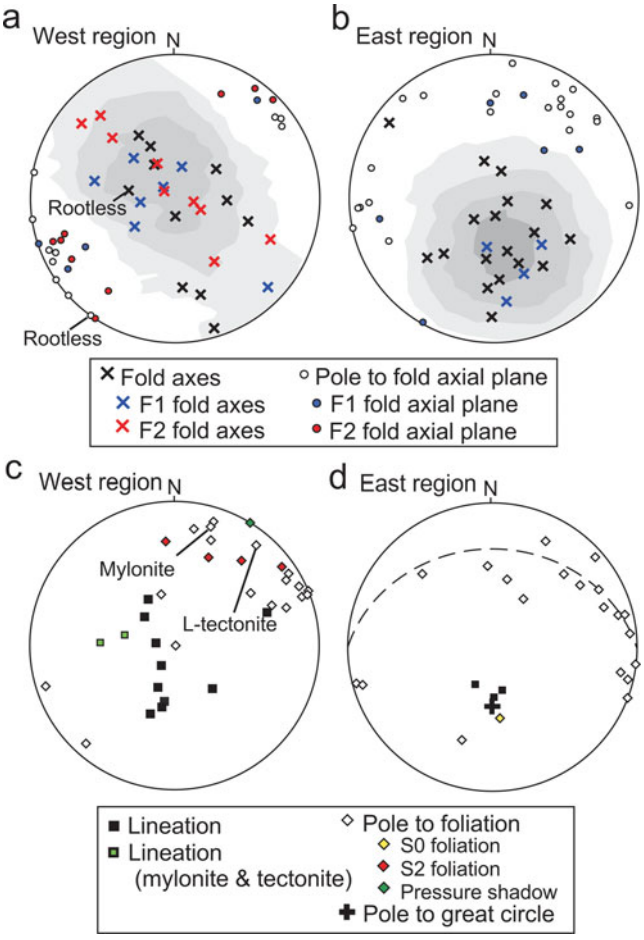

Fig. 5. Structural data from Akebono Rock. **a. & b.** Measured fold axes showing different trends between the east and west regions. Fold axes in the west regions lie along a NW-SE plane and variably plunge vertically to near horizontally. Grey shading represents Kamb contours (counter interval = 2.0 σ). **c. & d.** Foliation and mineral lineation (hornblende and quartz) in the east and west regions. Data of distinguishable foliation of S0/S1 and S2 are plotted as different markers. Data of 'pressure shadow' are identical to 'S3' in Fig.4e. '+' indicates the pole of the great circle deduced from the pole to foliation.

Among the various folds developed in the west region, one set is correlated with the F1 folds of the east region on the basis that they also contain clusters of unaltered garnets in their limbs and hinges. The migmatite and host gneisses commonly preserve S1 flattened foliation, which indicates D1 compression post-dating the leucosome emplacement (Fig. 3e). Later pegmatite veins (Fig. 3f) intrude the migmatites and the amphibolites, broadly sub-paralleling the amphibolite foliation (Fig. 3f).

Late deformation of Akebono Rock

The second deformation (D2) is characterized by the development of isoclinal to tight folds accompanied by an axial planar foliation (S2). In the west region of Akebono Rock, intrafolial, asymmetric, isoclinal to tight folds (F2) refold the S1 foliation (Fig. 3g & h). Examples exist where refolded F1 folds are included in the F2 fold hinge (Fig. 3h). F2 axial planes strike NW-SE and dip very steeply to the NE and SW (Fig. 5a), while the fold axes vary from vertical to near horizontal. Clustering distributions of poles to the F2 fold axial planes show a similar trend of NNE-SSW, as with those of the regional foliations in the west region of Akebono Rock.

An S2 fabric lies subparallel to the F2 fold axial planes. S2 foliation is characterized by the presence of asymmetric micro-textures, which are possibly synchronously formed by F2 folding. The north-dipping axial plane of the F2 fold (Fig. 5a) does not completely fit with the foliation data. Some indistinguishable axial plane folds (F2 folding?) in the east region (data are represented as open circles in Fig. 5b) are almost concordant with regional foliation in the west region. In places, this is marked by preferential alignment of biotite flakes as planer deformation fabric, for example, in Grt-leucogranite (Fig. 4c); in others, it is more of a finely spaced foliation (Fig. 4a & b). Within garnet-bearing gneiss and amphibolite, biotite and hornblende of the S2 fabric are developed around the garnets as a pressure shadow. S2 foliation suggests a sense of reverse fault motion to the shearing (Fig. 5d). The garnet-bearing leucogranite also has a similar texture and weak alignment of biotite; hence, it was influenced by the D2 deformation (Fig. 4c). The trend of S2 foliation varies from NW-SE to W-E.

Deformation along the shear zone

As pointed out previously, Hiroi *et al.* (1986) mapped a large shear zone that cuts almost E-W across the west region (Fig. 2). From this shear zone, we have collected samples that display mylonite (122902) and L-tectonite (122905) fabrics, with lineations defined by elongation of quartz and amphibole grains. A lineation is clearly defined in the L-tectonite by amphiboles, plunging moderately to the west, but there is also a weak foliation formed by biotite flake alignment. The mylonite foliation dips steeply to the south (Fig. 4d). The axes of rootless folds (Fig. 5a & c) parallel the moderate westward plunge of the lineation. The asymmetry of winged garnet porphyroclast in the mylonite, largely replaced by secondary biotite and muscovite, indicates a right-lateral sense of motion to the shear zone. Both the L-tectonite and mylonite fabrics indicate that the shear zone is inferred as a normal shear with downthrow to the south with a minor right lateral component (Fig. 6). In the outcrop, foliation associated with garnet pressure shadows is notably oblique to the S2 foliation (Fig. 4e) and is clearly related to the mylonite and L-tectonite fabrics (Fig. 5c).

https://doi.org/10.1017/S0954102020000450 Published online by Cambridge University Press

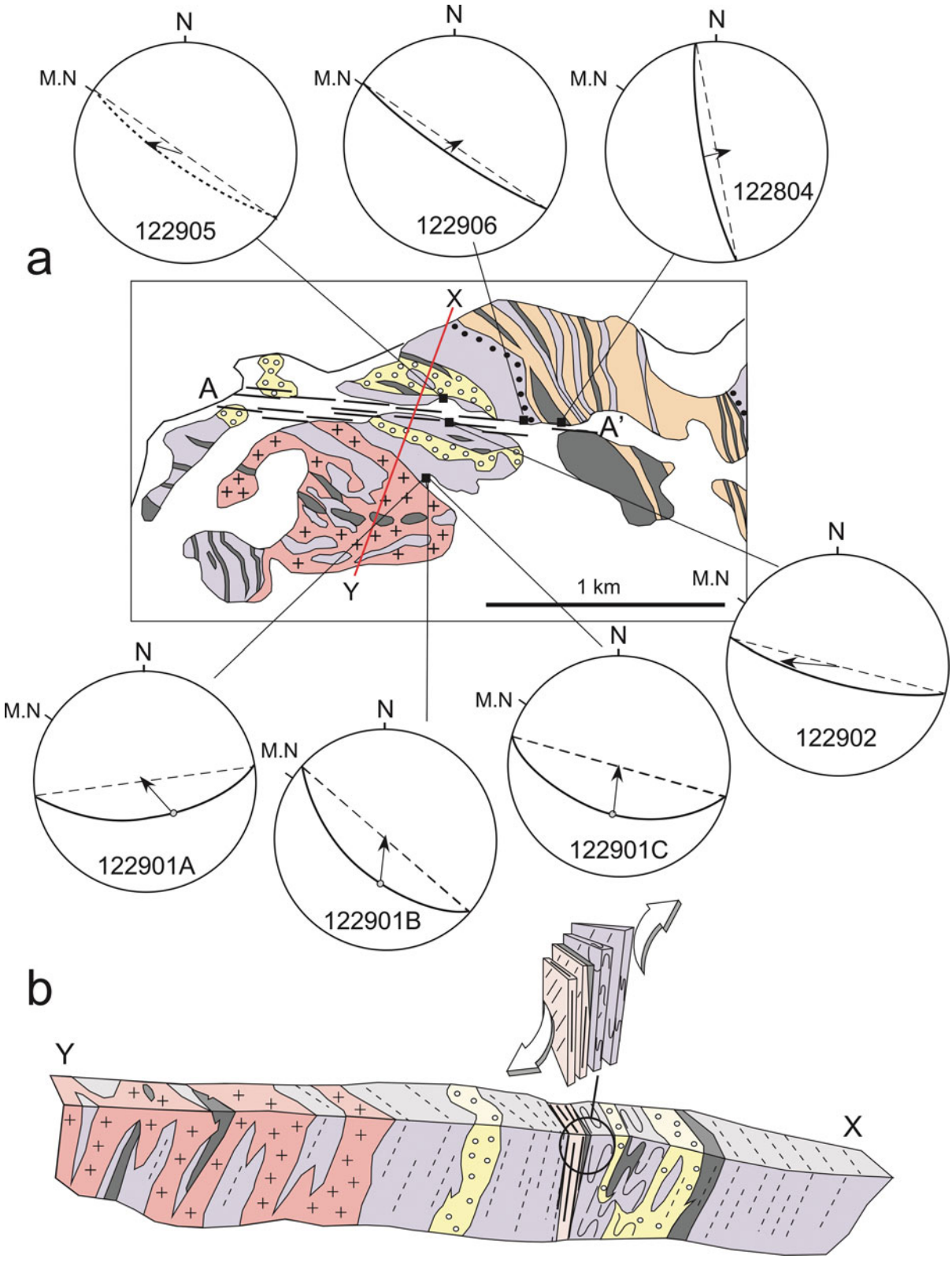

Fig. 6. a. Sense of shear deduced from asymmetric fabric in the orientated samples along the shear zone. Asymmetric fabrics formed by secondary biotite replacing garnet indicate reverse slip fault with top to north movement. Mylonite and tectonite show an oblique normal slip fault with right-lateral motion. **b.** Schematic image of mylonite and tectonite. M.N = magnetic north.

https://doi.org/10.1017/S0954102020000450 Published online by Cambridge University Press

Large garnet porphyroblasts are found in the amphibolites close to the shear zone (Fig. 4g). In many cases, these garnet grains have pressure shadows consisting of quartz and minor plagioclase. Occasionally, sigmoidal inclusion trails in such garnets are obvious in hand specimens, especially where Grt-amphibolite is enclosed by Grt-leucogranite (Fig. 4h).

Sampling and methods of analysis

Analysed samples were collected from the west region of Akebono Rock. All samples were collected as orientated and, from each of them, two standard thin sections were made perpendicular to the foliation: one parallel to and the other perpendicular to the lineation. The sense of shear motion was determined by using textural indicators as proposed by Passchier & Trouw (1996). The chemical composition of the minerals in these samples was analysed using a wavelength-dispersive electron microprobe (JEOL JXA-8800M) at the National Institute of Polar Research (Japan), with natural silicates and synthetic oxides as standards, an accelerating voltage of 15 kV and a beam current of 12–15 nA. ZAF correction was applied to the analysis and corrected element contents were recalculated to weight percent. Total iron is reported as FeO^T. Representative mineral compositions are listed in Tables SI–SIV.

Microstructures and mineral chemistry

In many of the Grt-bearing gneisses in the west region, secondary biotite forms asymmetric tails to the garnets (Fig. 7a). As discussed above, this texture is believed to have formed during D2. In general, the S2 consists of fine layers formed by ribbon quartz and secondary muscovite and K-feldspar (Fig. 7b). From orientated samples, the asymmetry of mica fish with S2 foliation and the biotite tails around garnet indicate that S2 formed during reverse fault movement (Fig. 6: 2901A, 2901B, 2901C, 2804 and 2906). However, in two samples, which are highly deformed, the textures indicate the opposite sense of shear motion, indicating that the shear zone may have experienced multiple episodes of movement.

Composition of minerals forming mylonite and L-tectonite textures

Sample 2902 is an intensely deformed Grt-bearing mylonitic gneiss (Fig. 7c). It consists of quartz, K-feldspar, plagioclase, muscovite, biotite and garnet with chlorite, zircon and ilmenite. There are alternating quartz-rich felsic, biotite + muscovite and fine-grained muscovite + quartz + plagioclase layers. The garnet porphyroblasts are partially replaced by muscovite and biotite along cracks that appear to be Riedel shear planes (Figs. 7d & e). The fragmented garnets form ellipsoidal domains, with asymmetric biotite wings. Garnet compositions are almost homogeneous (almandine 0.84–0.86, pyrope 0.07–0.09, grossular 0.02–0.03, spessartine 0.02–0.04). Biotite, which occurs as flakes surrounded by muscovite in the biotite + muscovite layers, has X_{Mg} values ranging from 0.27 to 0.34 and TiO_2 contents in the range of 1.95–3.70 wt.%. The TiO_2 content is highest in the cores of the largest biotite flakes in the matrix. Muscovite has TiO_2 contents of 0.55–1.11 wt.% and Si^{4+} contents of 6.19–6.39 atoms per formula unit (APFU) based on 22 oxygens. Plagioclase compositions have anorthite contents (An) in the range of 0.17–0.21. There is a small amount of presumably retrogressive chlorite that replaces muscovite and biotite.

Sample 2905 is an L-tectonite and consists chiefly of hornblende, plagioclase, biotite, quartz and garnet. Ilmenite, apatite and titanite are present as accessory minerals (Fig. 7f–i). Hornblende is magnesio-hornblende in composition and occurs as elongated grains, with a maximum aspect ratio of ~1:10 (Fig. 7g). The hornblende colour is predominantly greenish, although sometimes the inner parts have a brownish colour. Hornblende X_{Mg} values range from 0.64 to 0.69, with Ti contents of 0.09–0.14 APFU and A-site occupancy of 0.22–0.35 APFU. Despite the colour variation, there is no significant compositional difference between the cores and rims of individual grains. Plagioclase has numerous blebby quartz inclusions and shows distinct optical zoning with Na-richer cores (An 0.49–0.65) and Ca-rich rims (An 0.79–0.84). Biotite, which is less abundant than hornblende, is also elongated and has a homogeneous composition, with X_{Mg} values ranging from 0.60 to 0.30, and TiO_2 contents in the range 2.40–2.69 wt.%. Minor garnets, with anhedral columnar shapes, contain elongated ilmenite and quartz inclusion trails that parallel the external hornblende elongation (Fig. 7h & i). The garnet composition is usually fairly homogeneous (almandine 0.64–0.68, pyrope 0.13–0.18, grossular 0.14–0.20, spessartine 0.03–0.04); however, in the largest garnets, the cores have high pyrope and low grossular and almandine contents.

Mineral compositions and textures in garnet-amphibolites

Sample 2904B consists of hornblende, garnet, plagioclase, quartz, ilmenite and titanite. The garnets are euhedral and up to 30 mm in size. The garnet cores have randomly orientated fine-grained ilmenite, quartz and plagioclase inclusions, while in the rims there are elongate ilmenite inclusions that are parallel with the external foliation (Fig. 8a). The core and the rim are divided by a domain rich in coarse-grained quartz inclusions. Asymmetric

https://doi.org/10.1017/S0954102020000450 Published online by Cambridge University Press

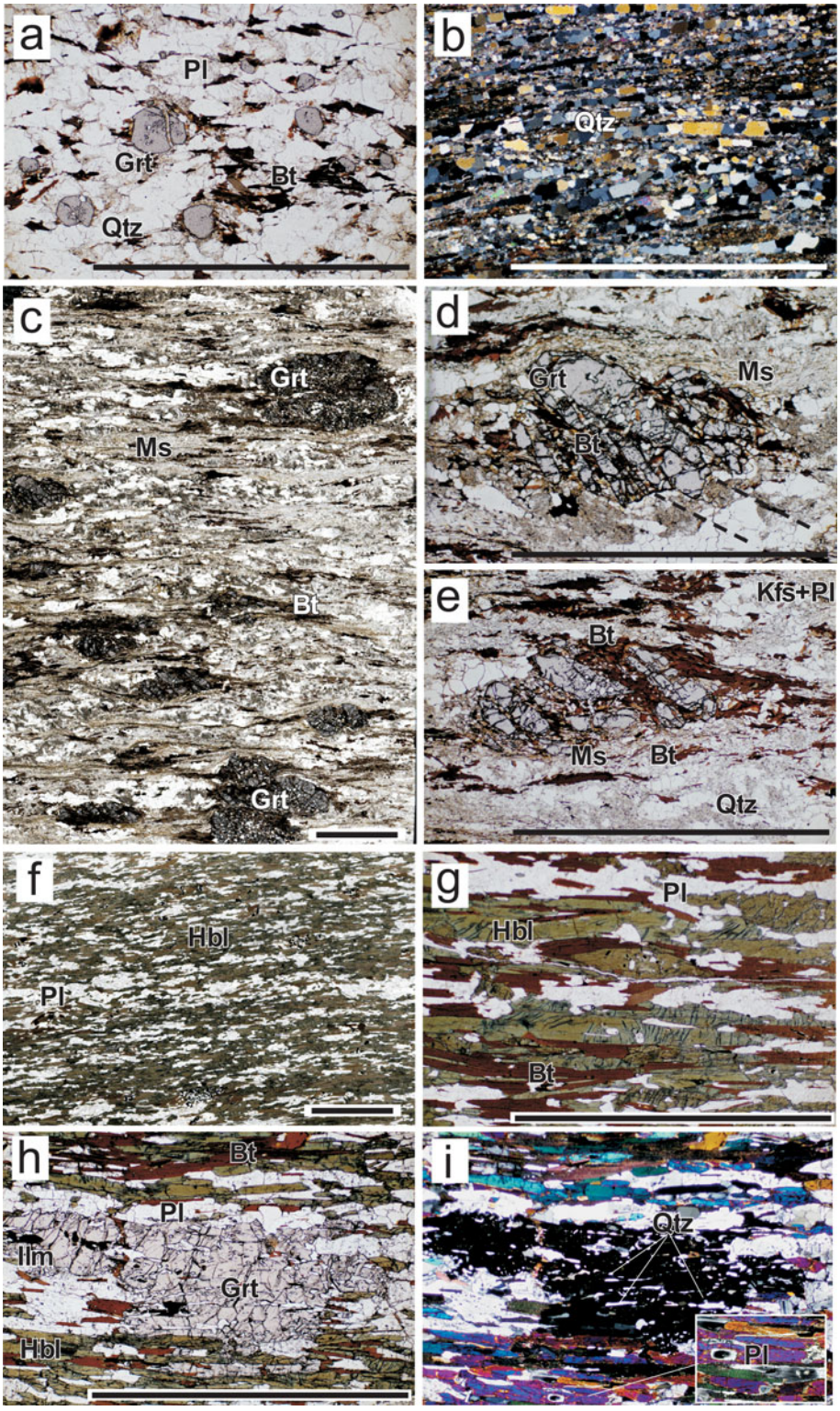

Fig. 7. Photomicrographs of mylonite and L-tectonite textures. **a.** Sample 2901B, garnet is replaced by secondary biotite that forms in pressure shadows and indicates the S2 foliation. **b.** Sample 2906, ribbon quartz is developed in the feldspathic domain (crossed polars). **c.–e.** Sample 2902, garnet breaks down to form secondary muscovite and biotite along the garnet cracks that have formed parallel to the Riedel shears. **f. & g.** Sample 2905, elongated grains of magnesio-hornblende with a maximum aspect ratio of ~1:10. **h.** Sample 2905, elongated garnet grains including elongated quartz inclusion trails parallel to the external foliation. **i.** Sample 2905, close-up view of plagioclase.

https://doi.org/10.1017/S0954102020000450 Published online by Cambridge University Press

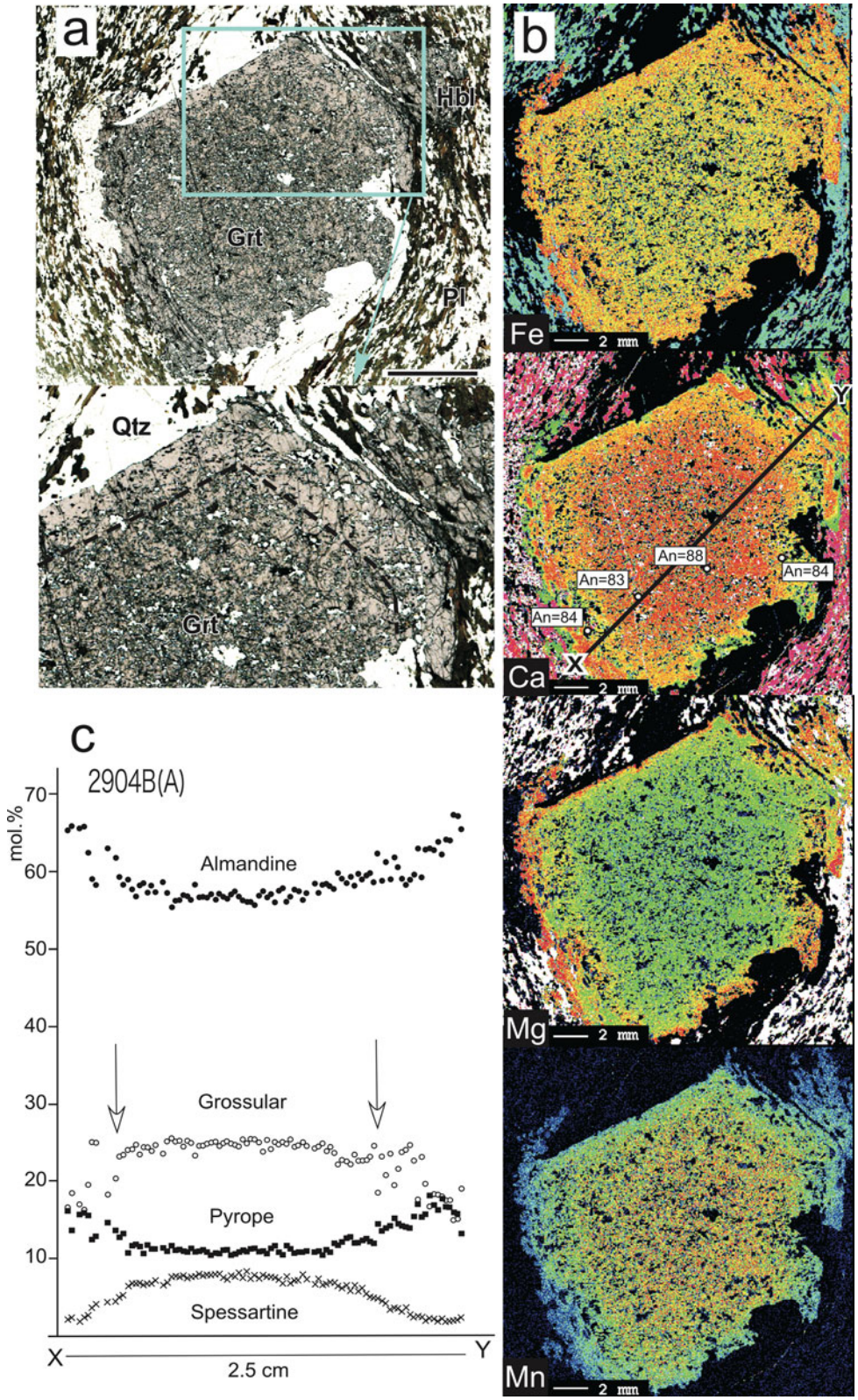

Fig. 8. Sample 2904B. **a.** Photomicrograph (scale bar 5 mm) showing large euhedral garnets with cores containing randomly orientated, fine-grained ilmenite, quartz and plagioclase inclusions, whilst rims have elongated ilmenite inclusions that are parallel to the external foliation. **b.** Maps of X-ray intensity of Fe, Ca, Mg and Mn for the upper garnet porphyroblast. **c.** Chemical zoning profiles of the upper garnet porphyroblast (line of traverse) shown on the Ca X-ray intensity map.

https://doi.org/10.1017/S0954102020000450 Published online by Cambridge University Press

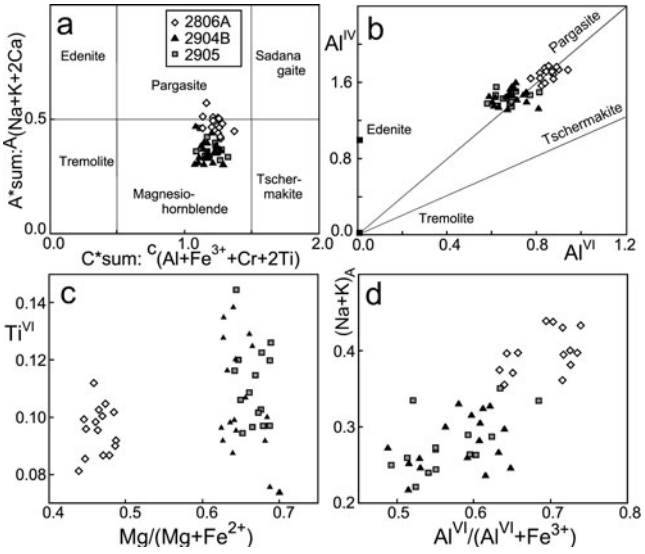

Fig. 9. Compositional variations of hornblende. Data were recalculated using *ACE* v.1.93. (Locock 2014). **a.** Calcium amphiboles and their compositional boundaries are after Hawthorne *et al.* (2012). **b.** Variation of Al^{IV} with Al^{VI}. **c.** Variation of Ti^{VI} with $Mg/(Mg + Fe^{2+})$. **d.** Variation of $(Na + K)^{A}$ with $Al^{VI}/(Al^{VI} + Fe^{3+})$ content.

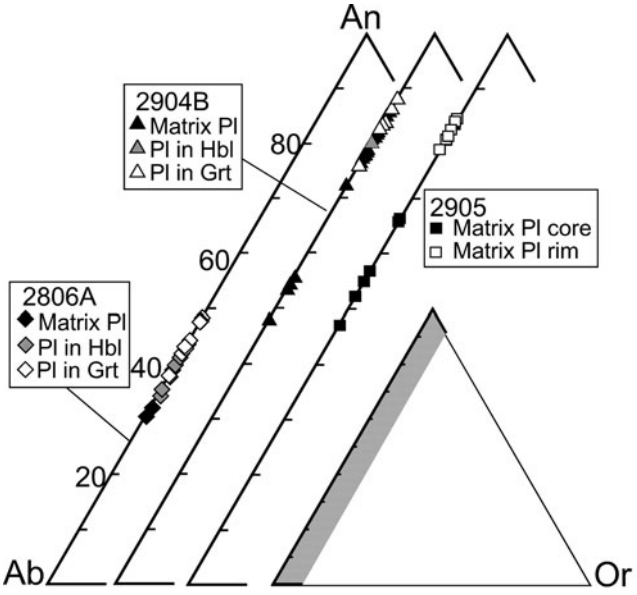

Fig. 10. Compositional variation of plagioclase in terms of An-Ab-Or ternary diagrams.

pressure shadows around the garnets are composed mainly of quartz. The garnets are compositionally zoned (Fig. 8b & c), with a decrease in spessartine and grossular content from core to the rim (spessartine 0.08 to 0.02; grossular 0.25 to 0.15) and an increase in pyrope and almandine content from core to rim (pyrope 0.10 to 0.17, almandine 0.56 to 0.67). The inclusion-rich core is relatively homogeneous in composition, whiles the rims have higher pyrope and almandine contents (up to 0.17 and 0.67, respectively). While there is a general decrease (25 to 15) in grossular content from the inside to the outside of the rim, the pattern is not smooth (Fig. 8c). The amphibole is a magnesio-hornblende (Fig. 9) and shows X_{Mg} values in the range of 0.62–0.70, with Ti contents of 0.07–0.14 APFU and A-site occupancy of 0.19–0.33 APFU. Plagioclase inclusions within the garnet have a high anorthite content of 0.83–0.88. In contrast, matrix plagioclase shows distinctive zoning, the core is lower in An (0.55) than the rims (0.73–0.79) (Fig. 10).

Sample 2806A consists of hornblende, plagioclase, garnet, quartz, biotite and ilmenite with accessory apatite and titanite. It contains a large garnet with S-shaped inclusion trails ($S2_{-2}$) in the core and Z-shaped inclusion trails ($S2_{-1}$) in the rim (Fig. 11a). The latter inclusion trails are continued with the matrix foliation. The garnet shows weak compositional zoning, with a decrease in spessartine and grossular and an increase in almandine towards the rim, with a clear discontinuity in the compositional zoning profile (Fig. 11b & c). These spikiness of the compositional profile suggests a modification of the garnet compositions during the growth in relation to the rotation (Fig. 11c). The amphibole is magnesio-hornblende to pargasite in composition (Fig. 9) and has X_{Mg} values in the range of 0.44–0.48, with Ti contents of 0.09–0.11 APFU and A-site occupancy of 0.36–0.44 APFU. The matrix plagioclase composition (Fig. 10) is lower in An (0.32–0.44) compared to inclusions in the garnet (0.42–0.48). Plagioclase inclusions within hornblendes have similar An (0.34–0.43) to those in the matrix.

Metamorphic conditions

The equilibrium *P-T* conditions during the metamorphism associated with deformation were estimated by using experimentally calibrated geothermobarometers based on the systems of Hbl-Pl (Holland & Blundy 1994), Grt-Bt (Hodges & Spear 1982, Bhattacharya *et al.* 1992, Holdaway 2000), Grt-Hbl-Pl-Qtz (Kohn & Spear 1990), Grt-Ms-Bt-Pl-Qtz (Wu & Zhao 2007) and Grt-Bt-Pl-Qtz (Hoisch 1990). We did not apply isochemical phase modelling (pseudosection) because the highly deformed rock was affected by retrograde hydration, indicating that the presence of water would affect the stability fields in the phase diagrams.

To estimate peak *P-T* conditions, we used the composition of the high-Mg garnet rim together with matrix plagioclase and matrix hornblende. We carried out the calculations using both high-X_{An} and low-X_{An} zones of matrix plagioclase grains to assess the range

https://doi.org/10.1017/S0954102020000450 Published online by Cambridge University Press

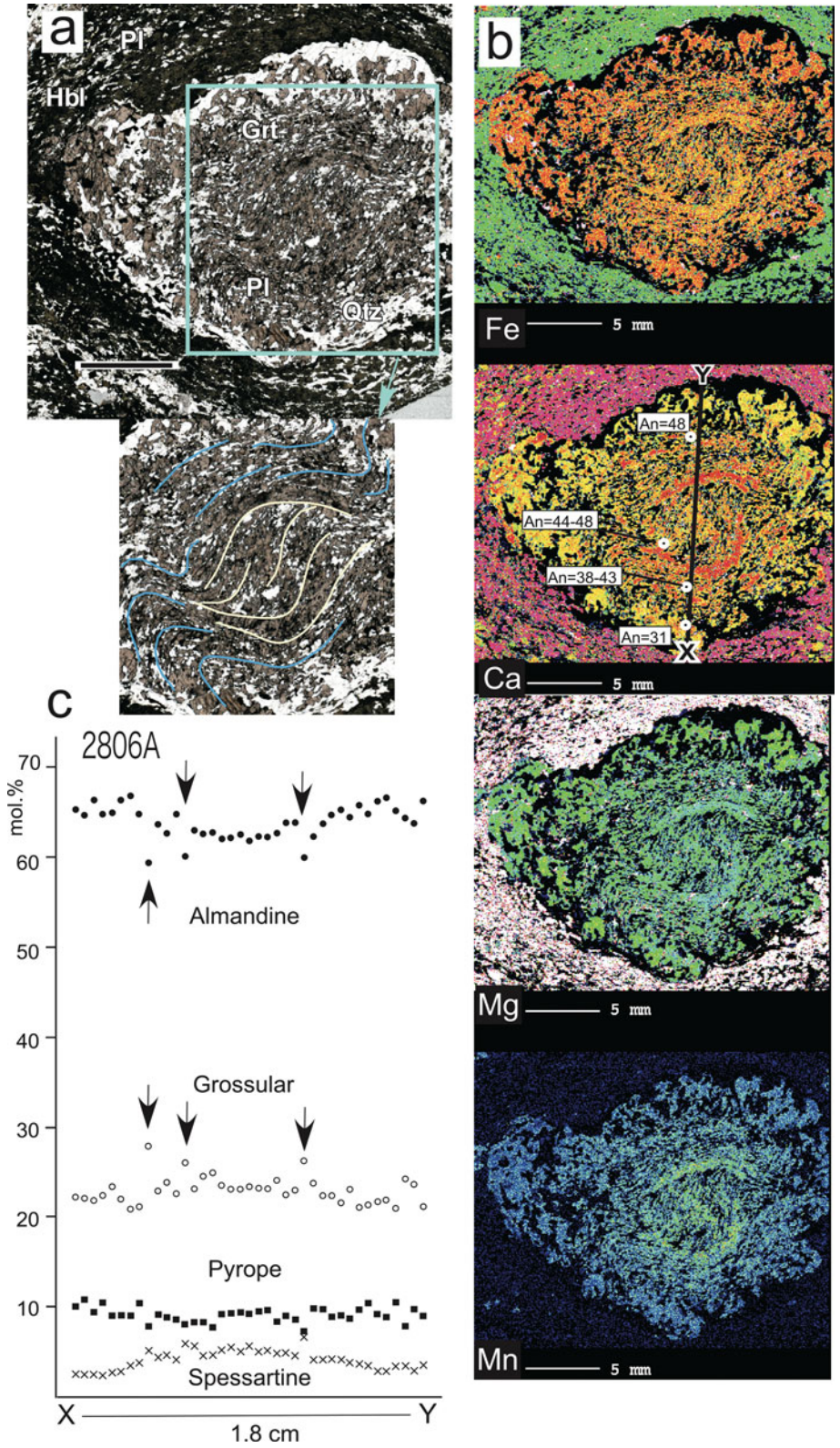

Fig. 11. Sample 2806A. **a.** Photomicrograph (scale bar 5 mm) of a garnet with a core of S-shaped inclusion trails and a rim with Z-shaped inclusion trails. **b.** Maps of X-ray intensity of the Fe, Ca, Mg and Mn for this double sigmoidal garnet. The extent of the core domain with S-shaped inclusion trails is clearly imaged. **c.** Chemical zoning profiles of this garnet (traverse indicated by the solid line in the Ca X-ray intensity map).

https://doi.org/10.1017/S0954102020000450 Published online by Cambridge University Press

Table I. Thermobarometric results for Grt-Hbl-Pl-Qtz associations.

Sample	Note	Spot no.	Grt-Hbl-Pl	*T* (at 4 kbar) (°C)		*T* (at 7 kbar) (°C)		*P* (at 600°C) (kbar)			*P* (at 700°C) (kbar)		
				HB1	HB2	HB1	HB2	KS1	KS2	Av.	KS1	KS2	Av.
2806A	Sigmoidal	50-40-46	r-mtx-mtx	659	618	691	659	7.8	7.7	7.7	8.5	7.9	8.2
2806A	Sigmoidal	36-31-38	r-mtx-mtx	629	606	657	655	7.5	7.4	7.5	8.3	7.6	7.9
2806A	Sigmoidal	70-73-76	r-mtx-in Hbl	644	636	667	672	7.9	7.6	7.7	8.7	7.8	8.2
2806A	Sigmoidal	71-67-83	r-mtxr-mtx	636	614	662	652	7.4	7.0	7.2	8.2	7.2	7.7
806A	Sigmoidal	52-41-47	r-mtx-mtx	636	625	659	662	8.0	8.0	8.0	8.9	8.2	8.5
2904B	Euhedral	99-92-90	r-mtx-mtx	688	734	705	776	4.9	3.7	4.3	5.3	3.5	4.4
2904B	Euhedral	101-91-87	m-mtx-mtx	697	718	709	751	6.9	5.9	6.4	7.6	5.9	6.7
2904B	Euhedral	113-127-115	r-mtx-mtx	652	698	668	739	4.6	3.2	3.9	4.9	2.9	3.9
2904B	Euhedral	97-95-88	r-mtx-mtx	720	735	725	768	5.5	4.0	4.7	6.0	3.7	4.8
2905	Tectonite	13-7-22	r-mtx-mtx r	740	736	755	774	4.4	3.0	3.7	4.8	2.6	3.7
2905	Tectonite	18-8-21	c-mtx-mtx c	665	684	676	717	6.3	5.4	5.9	6.9	5.3	6.1
2905	Tectonite	32.5-31-30	r-mtx-mtx r	742	781	745	814	5.3	3.5	4.4	5.7	3.2	4.5
2905	Tectonite	39-26-28	c-mtx-mtx	658	712	666	746	5.3	3.7	4.5	5.7	3.4	4.5

HB1 = equation A (Qtz-present) in Holland & Blundy (1994), HB2 = equation B (Qtz-absent) in Holland & Blundy (1994), KS1 = tschermakite-Fe model in Kohn & Spear (1990), KS2 = tschermakite-Mg model in Kohn & Spear (1990), r = rim, mtx = matrix, c = core, Av. = average.

of pressure conditions (Tables I & II). Temperatures calculated using the Hbl-Pl thermometer (HB1: equation A in Holland & Blundy 1994) range from 629°C to 742°C, assuming a pressure of 4 kbar. The highest temperature was obtained from the L-tectonite (sample 2905) when using the composition of a high-X_{An} plagioclase rim. Pressures calculated using the Grt-Hbl-Pl-Qtz barometry (KS2: tschermakite-Mg models: Kohn & Spear 1990) range from 3.0 to 8.0 kbar. The highest pressure (~8.0 kbar at 600°C) was obtained from the sigmoidal Grt-bearing amphibolite (sample 2806A) and is significantly higher than those of the other two samples (~6.4 kbar at 600°C).

For the biotite-bearing sample 2902, *P-T* estimates obtained from a variety of methods are summarized in Fig. 12. According to the recommendation by Wu & Chen (2006), temperatures obtained using the Grt-Bt thermometer by Holdaway (2000) range from 611°C to 658°C at 4 kbar. Pressures calculated using the Grt-Bt-Pl-Qtz barometry (Hoisch 1990) range from 3.8 to 4.4 kbar at 600°C. Grt-Ms-Bt-Pl-Qtz barometry (Wu & Zhao 2007) gave similar values (4.2 kbar at 600°C: Sil model).

Discussion

Deformation history

Table III summarizes the deformation history of Akebono Rock. A pervasive gneissic foliation is the main fabric of most lithological units, and original igneous or sedimentary contacts cannot be distinguished. The first deformation episode of the gnessic fabric (D1) produced somewhat chaotic flow folding (F1), indicating that it took place under ductile conditions. A set of leucocratic veins appears to be concordant with the F1 folds, suggesting that they were intruded either prior to or synchronous with the D1 event. The development of a weak S1 subparallel to the F1 axial planes it taken to indicate that, during flow folding, the maximum compressive force was orthogonal to the axial planes. More competent beds were also boudinaged during D1. Outcrop-scale F1 folds are probably parasitic to a large, open, map-scale fold (Fig. 2), as indicated by the fact that the pole of the great circle obtained by the regional foliation in the east region is consistent with the maximum concentration of the F1 fold axes (Fig. 5b). During D1, garnet appears to have been a stable phase.

Table II. Thermobarometric results for Grt-Bt-Pl-Qtz associations.

Sample	Note	Spot no.	Grt-Bt-Pl	*T* (at 4 kbar) (°C)			*T* (at 7 kbar) (°C)			*P* (at 600°C) (kbar)			*P* (at 700°C) (kbar)		
				HO	HS	B92b	HO	HS	B92b	Wu07a	Wu07b	Hoi	Wu07a	Wu07b	Hoi
2902	Mylonite	70-71-74	r-rep-in rep	658	694	626	668	707	629	6.6	4.2	4.3	9.0	6.1	6.0
2902	Mylonite	94-95-103	r-rep-mtx	611	600	578	619	612	581	-	-	4.3	-	-	6.1
2902	Mylonite	104-105-106	r-rep-mtx	637	659	612	645	671	615	-	-	4.2	-	-	5.9
2902	Mylonite	110-119-136	c-rep-mtx	615	613	589	624	625	591	-	-	3.8	-	-	5.5
2902	Mylonite	123-124-125	r-rep-mtx	636	660	613	645	673	616	-	-	4.4	-	-	6.2
2902	Mylonite	131-141-146	c-rep-mtx	640	677	626	649	685	629	-	-	4.2	-	-	5.9

HO = Holdaway (2000), HS = Hodge & Spear (1982), B92b = Bhattacharya *et al.* (1992: Ganguly and Saxena garnet model), Wu07a = Wu & Zhao (2007: Ky model), Wu07b = Wu & Zhao (2007: Sil model), Hoi = Hoisch (1990: Fe end-member model), r = rim, rep = replaced grain, in rep = in side of replaced texture, mtx = matrix.

https://doi.org/10.1017/S0954102020000450 Published online by Cambridge University Press

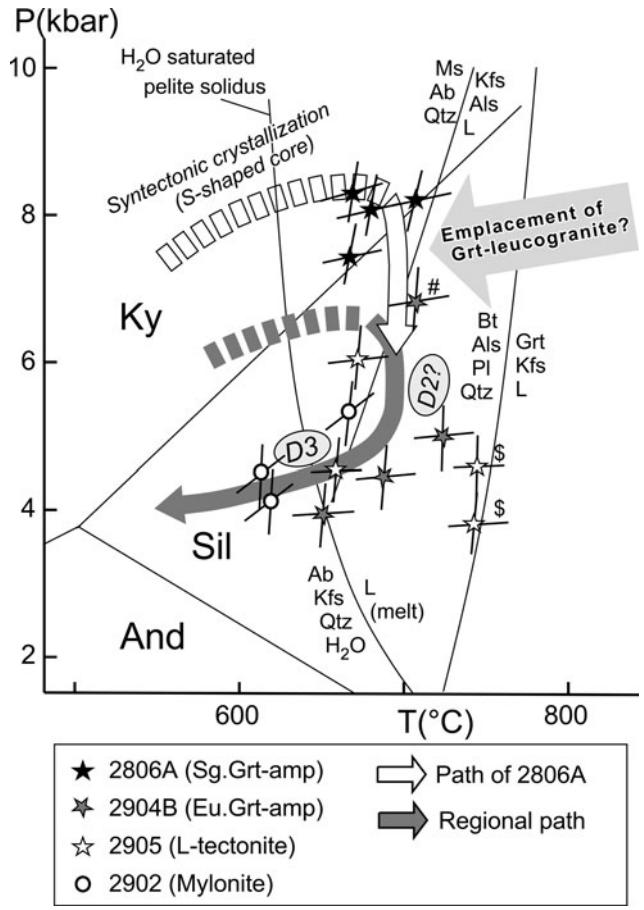

Fig. 12. Inferred *P-T-d* paths for sigmoidal garnet-bearing amphibolite (white path) and mylonite, L-tectonite and other Grt-amphibolites (grey path), showing deeper, higher-pressure metamorphism of the sigmoidal garnet-bearing amphibolite and subsequent decompressive isothermal uplift bringing it into contact with the other lithological units of Akebono Rock. Melting reactions were taken from Le Breton & Thompson (1988).

The second deformation (D2) is characterized by the F2 fold, and S2 fabric (Fig. 7a) lies subparallel to the F2 fold axial planes. The fact that F2 fold axes plotted on a stereonet (Fig. 5a) lie on a great circle implies that they have been refolded around a NE-SW trending younger fold. However, no such younger fold has been identified in the field. The fold axes are not well clustered, and the distribution patterns of the fold axes resemble those of sheath fold (e.g. Talarico *et al.* 2007). In the field, a non-cylindrical fold was found (Fig. 4a); therefore, a superimposed structure (e.g. bending of the fold axis by the shearing) is assumed. A north-dipping axial plane of the F2 fold (Fig. 5a) does not completely fit with the S2 foliation data in the west region, but fits well with the regional foliation in the east region. This inconsistency may have been caused by the modification of the subsequent deformation in the west region. As a result, the dip angle of the fold axial plane in the west region is assumed to change from moderately dipping to a high angle.

The third deformation (D3) is activation of the shear zone to form mylonite and L-tectonite foliations (S3). This shear zone may, in fact, have been active previously and responsible for uplifting and emplacing the sigmoidal Gnt-amphibolite, which appears to have been initially metamorphosed at a greater depth (~8.0 kbar) than other lithologies (~6.4 kbar) of Akebono Rock. Orientated samples indicate that, similar to D2, the motion of the D3 phase of the shear zone was also oblique normal slip, accompanied by right-lateral motion. However, unlike S2, the D3 fabrics are characterized by muscovite as a stable mineral. S3 is characterized by S/C fabrics, as shown in Fig. 7c–e. Where the deformation is more intense, garnets have been fragmented and drawn out into lensoidal shapes, cut by a set of fractures corresponding to Riedel shears. In other places, garnets have remained intact, with the development of asymmetric pressure shadows and wings, providing indicators of the direction of shear (Fig. 4f). Generally, D3 deformation has been intense enough to completely modify the S2 fabric, shearing it to become parallel with S3 and drawing out F2 folds so that they become rootless and non-cylindrical. However, in a low-strained zone, the S3 foliation (mylonite) can be seen to be at an angle of ~20° to S2 (Fig. 4e).

There are minor fabrics that are restricted to the vicinity of the pegmatite and Grt-leucogranite, and these appear to be directly related to their emplacement. In the limited time available in the field, we were unable to decide whether this deformation was related to either the D2 or D3 event. It is also possible that the emplacement of the Grt-leucogranite accompanied by planer fabric was an event intermediate between D2 and D3.

Characterization of the shear zone

Asymmetric fabrics observed within both the mylonite and L-tectonite suggest that within this shear zone the overall movement was one of oblique normal slip with right-lateral motion (Fig. 6: 2902, 2905). In the mylonites, garnet rims are partially replaced by secondary biotite and muscovite that extend into asymmetric wings in the matrix. Secondary biotite and muscovite also develop along with fractures in the garnets, the orientation of which relative to the matrix schistosity is consistent with them having formed as Riedel shears. Systematic orientated garnet cracks suggest that the garnet has deformed in a brittle manner, whereas the matrix deforms in a ductile manner. The formation of secondary muscovite and biotite after garnet and within the matrix suggests the infiltration of a limited amount of H_2O-rich fluid during retrogression, at the same time as D2 deformation was taking place.

https://doi.org/10.1017/S0954102020000450 Published online by Cambridge University Press

Table III. Preliminary history of the development of structural elements in Akebono Rock.

		West region	East region
D3	F3	Rootless fold by shearing and modification of F2 fold	-
Shearing 2	S3	Formation of mylonite and tectonite (Grt replaced by Bt + Ms)	-
D2	F2	Tight to isoclinal fold (Bt in axial plane)	
Shearing 1	S2	Foliation with asymmetric fabric (Grt replaced by Bt)	
Magmatism		Emplacement of Grt-leucogranite	
	$S2_{-1}$, $S2_{-2}$	Syntectonic crystallization of sigmoidal garnet core and rim in Grt-amphibolite	
Magmatism		Emplacement of pegmatite and pink granite	
Magmatism		-	Amphibolite II
D1	F1	Flow fold (Grt stable)	
Compression	S1	Boudinage and S1 foliation	
		Emplacement of leucosome	
D0			
Loading	S0	Formation of compositional banding of gneisses and amphibolite I	

S0 = primary gneissic foliation; S1: flattened foliation, S2 = secondary foliation associated with shearing, $S2_{-1}$ and $S2_{-2}$: inclusion trails for the rim and core, S3 = mylonite and weak foliation in L-tectonite.

The L-tectonite is characterized by elongated hornblende with aspect ratios of up to 1:10. In some cases, there are anhedral columnar garnets, with inclusions of elongate quartz grains that parallel the lineation of the hornblendes (Fig. 7i). Such garnets have homogeneous compositions, which suggests that they probably formed by complete recrystallization synchronous with the deformation. Matrix plagioclase shows distinctive compositional zoning, with a high anorthite rim, which probably reflects the breakdown of calcium-rich minerals, such as grossular garnet, during this retrogressive phase. The hornblende and plagioclase core compositions of L-tectonite are similar to those of matrix hornblende and plagioclase in the euhedral Grt-bearing amphibolite (2904B), respectively. On the basis of the compositional similarity, L-tectonite is considered to have derived from, and to have formed through an intense deformation it. The previous texture of the rock may have been completely erased by D3.

Estimated *P-T* conditions for the mylonite and L-tectonite are ~4.0–5.0 kbar, 610–660°C (Fig. 12: 2902) and 3.7–6.0 kbar, 660–740°C (Fig. 12: 2905), respectively. As for L-tectonite (2905), the high-temperature conditions of > 700°C (data indicated by '$' in Fig. 12) were obtained by using the plagioclase composition of the high-Ca rim. Except for these data, the *P-T* conditions of 610–660°C and 4–5 kbar are plausible for the stability of the minerals accompanying deformation, which essentially corresponds to the D3 stage (Fig. 12). The origin of these high-Ca rims in the L-tectonite is an enigma, but it is plausibly due to localized heating during deformation. A disequilibrium with the matrix minerals is an alternative explanation for this high temperature, but further discussion is beyond the scope of this paper.

The two types of garnet-amphibolites

At Akebono Rock, there are two types of Grt-amphibolites, which contain euhedral and sigmoidal garnet porphyroblasts, respectively. Although the primary mineral assemblages are the same for both types of Grt-amphibolite (garnet, hornblende and plagioclase), the chemical compositions of these phases are different. It is probable that this difference is inherited from their protolith compositions. At Akebono Rock, such sigmoidal garnets are only found close to the shear zone. It should be noted that sigmoidal garnet has not been reported previously from the other areas of the LHC. Sigmoidal rotated garnet is reported from collisional orogenic belts such as the Himalayas and Alps (e.g. Powell & Vernon 1979, Robyr *et al.* 2009) and is commonly interpreted as syntectonic growth.

The garnet grains in the sigmoidal Grt-amphibolite have S-shaped inclusion trails in the core and Z-shaped trails in the rims, the latter being continuous with the matrix fabric (Fig. 11a). In addition, the cores and rims have different compositions (Fig. 11b), and the profiles show a distinct break between the two (Fig. 11c). The element concentrations are concordant with the S-shaped inclusion trail (Fig. 11b). The sizes of the inclusions are much larger in the rim compared with the core. These textural and compositional features can be interpreted in two different ways. It is possible that they indicate two discrete phases of garnet growth, both of which being syntectonic. This could be due to two different metamorphic events. Alternatively, the cores and rims could correspond to two different garnet-producing reactions in the same prograde metamorphic event, with a change in the sense of shear occurring at the same time.

The external foliations around these garnet grains show asymmetric textures; therefore, they seem to be

https://doi.org/10.1017/S0954102020000450 Published online by Cambridge University Press

comparable to S2 foliation accompanied by an asymmetric pressure shadow around the garnet. However, Grt-amphiboles are enclosed in Grt-leucogranite and have a different orientation from the S2 foliation measured in the adjacent outcrop. This is considered to be the result of transposition due to enclosure by the Grt-leucogranite. The Grt-leucogranite foliation has the same orientation as the surrounding one, and the asymmetric texture of the garnet rim in the Grt-amphibolite is better considered as a shear plane prior to S2 ($S2_{-1}$). The S-shaped inclusion trail in the core is considered to be earlier than the rim due to dynamic crystallization ($S2_{-2}$) during the prograde metamorphism.

In contrast, the euhedral garnets found in other Grt-amphibolites show no evidence of any preferred orientation of inclusions in either their cores or rims, nor is there an obvious difference in the sizes of the inclusions between these two domains (Fig. 8a & b). The compositional difference between the cores and the rims, as evident from the profiles shown in Fig. 8c, is typical of garnets where the rims have re-equilibrated with the matrix assemblage during a later stage of a metamorphic event or during a retrograde event. The core compositions remain unaltered due to a slow rate of diffusion through garnet below a critical temperature. This is discussed further below.

P-T evolution of the Grt-amphibolites

The euhedral garnets show compositional zoning whereby, in comparison to their cores, their rims have lower grossular and spessartine contents, but higher pyrope and almandine contents (Fig. 8c). The *P-T* conditions using the rim composition of the garnet yield range from 650°C to 730°C and from 4 to 5 kbar. The estimated pressure condition is similar to that of the L-tectonite. Asymmetric deformation preserved in the rim of euhedral garnet (Fig. 8a) possibly occurred at a similar crustal level to the L-tectonite. Estimated *P-T* conditions using the garnet mantle and the low-An plagioclase in the matrix (data indicated by # in Fig. 12) are 700°C and 6.7 kbar, and these conditions represent the peak stage.

The compositional zoning of the sigmoidal garnet, as shown in the profile in Fig. 11c, is much more subdued between the core and rim. However, the profile does show a distinct change (see arrows in Fig. 11c) between the two domains, with values in the rim being somewhat erratic. A comparison of the profile and elemental maps (Fig. 11b & c) indicates that at least some of this erratic nature of the profile may be due to spiralling during growth, forming distinct compositional bands. Estimated *P-T* conditions using four sets of analysis points from the rim of garnets with adjacent matrix plagioclase and hornblende show a narrow *P-T* range of $\sim 8 \pm 0.3$ kbar and 650–700°C (Fig. 12: 2806A). These estimated *P-T* conditions are comparable with those of a kyanite-bearing garnet-biotite gneiss (650–700°C and 8 kbar) from north of the shear zone, which was analysed by Baba *et al.* (unpublished data 2017).

Figure 12 shows separate clockwise *P-T* paths for the sigmoidal Grt-amphibolite and the euhedral Gnt-amphibolite from the western part of Akebono Rock, based on the results of this study. From this, we postulate that the sigmoidal Grt-amphibolite was metamorphosed at significantly deeper crustal levels, corresponding to a peak pressure of ~8 kbar and a temperature of ~700°C (Fig. 12: white arrow). Our interpretation is that the core formed by syntectonic growth during the prograde metamorphism. Subsequently, this amphibolite became enclosed in a Grt-leucogranite, with the two of them then being brought to a shallower level corresponding to a pressure of ~6 kbar with the temperature maintained at 700°C, probably by movement related to early movement in the shear zone. It is possible that the garnet rims, with their opposite sense of rotation to the cores, were formed during this exhumation and isothermal decompression process. Deformation during this uplift corresponds to the D2 event, when the S2 foliation in the Grt-leucogranite was formed.

As for the euhedral Grt-amphibolite, this was metamorphosed at a shallower level, with peak pressure at ~6 kbar and a temperature of ~700°C (Fig. 12: grey arrow). Both types of amphibolite then continued to be uplifted and underwent retrograde metamorphism, although the degree of retrograde hydration reactions was limited by the available water. We believe that the D2 episode corresponds to this uplift phase. During the uplift and retrograde metamorphic phase, the shear zone appears to have been reactivated, representing the D3 event. This is evident from the fact that analysis of the associated mylonite and L-tectonite indicates that they were metamorphosed at 4 kbar and 650°C.

Regional correlation

The metamorphic grade of the LHC is considered to increase towards the south-west, with NNW-SSE trending isograds (Fig. 13). The shear zone at Akebono Rock trends E-W, thus it is oblique to these isograds. East of Akebono Rock towards Cape Ryûgû, the tectonic and metamorphic history is not well understood. At Cape Ryûgû, basement rocks, composed of muscovite-bearing biotite leucocratic gneiss and augen gneiss, have a general E-W structural trend (Nakai *et al.* 1980). The biotite leucocratic gneiss contains garnets and resembles the Grt-leucogranite found at Akebono Rock. The appearance of the augen gneiss implies the presence of the shear zone. Although it is tempting to assume a correlation between Akebono

https://doi.org/10.1017/S0954102020000450 Published online by Cambridge University Press

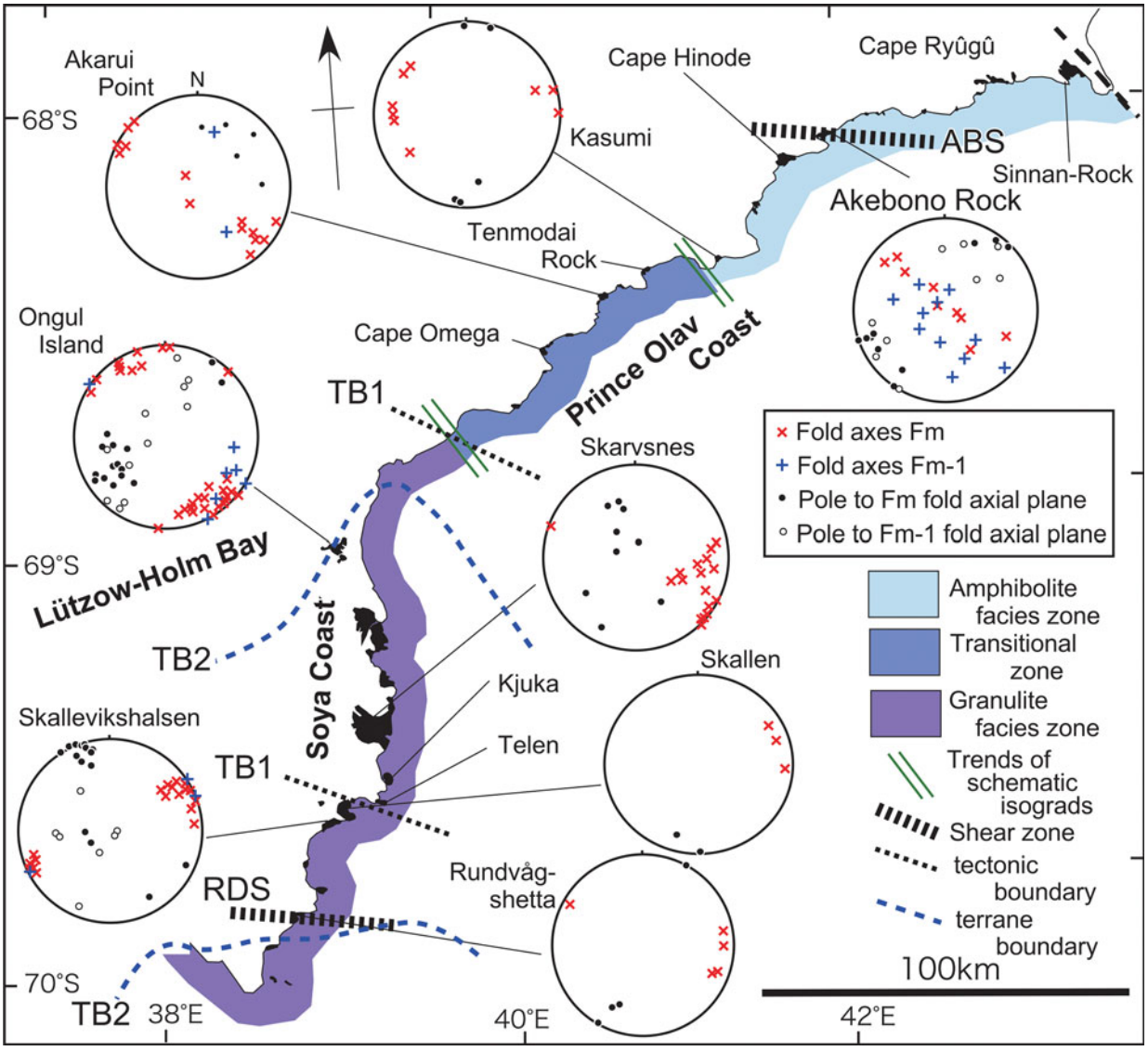

Fig. 13. Compiled map of structural data, major shear zone, schematic isograds (Hiroi *et al.* 1991) and tectonic boundaries in the Lützow-Holm Complex. Structural data are taken from Ikeda & Kawakami (2004 and reference therein). Distinguishable fold data (see Fig. 5) from Akebono Rock were plotted, and F1 and F2 are represented as Fm-1 and Fm. RDS = shear zone in Rundvågshetta (Ishikawa *et al.* 1994), ABS = shear zone in Akebono Rock (Hiroi *et al.* 1986 and this study), TB1 = tectonic boundary (modified after Yoshida 1979), TB2 = terrane boundary (modified after Takamura *et al.* 2018).

Rock and Cape Ryûgû based on this lithological similarity, such garnet-bearing leucocratic gneisses are common in many basement complexes. Such a correlation will have to wait until detailed structural and petrological studies are conducted at Cape Ryûgû, which has not been studied since 1978 (19th Japanese Antarctic Research Expedition).

With the exception of this study, there are no descriptions of shear-zone deformation and the resulting tectonites within the LHC along the Soya Coast. On the Soya Coast, some researchers postulated tectonic/terrane boundaries (Fig. 13), but the detailed occurrences of the tectonite are not understood. Ishikawa *et al.* (1994) describe high-strain ductile deformation producing isoclinal buckling folds (Fn) and boudinage during the peak granulite-facies metamorphism at Rundvågshetta (RDS in Fig. 13). Ishikawa *et al.* (1994) report ductile thrusting and minor extensional conjugate shear zones at Rundvågshetta, both occurring post-peak metamorphism, but they do not record any development of related tectonites. We are reluctant to propose any correlation between deformation structures found at Rundvågshetta and Akebono Rock, given their great distance of separation and different metamorphic grades.

Ikeda & Kawakami (2004) compiled structural data from seven localities in the LCH. They suggest that the

https://doi.org/10.1017/S0954102020000450 Published online by Cambridge University Press

axes of the main folding (Fm) trend NW-SE. In outcrops at Skarvsness, Ongul Islands and Akarui Point, the fold axes plunge at shallow angles towards the SE (Fig. 13). In contrast, the axes of the same fold set at Skallevikshalsen and Skallen trend ENE-WSW and plunge horizontally (Fig. 13). At Kasumi Rock, the fold axes appear to trend close to E-W, but there is considerable scatter in the data. The trends of both the F1 and F2 fold axes at Akebono Rock differ from the folds at the localities described by Ikeda & Kawakami (2004). It is possible that the F2 folds found at Akebono Rock correspond to the regional Fm folds of Ikeda & Kawakami (2004) and that their orientation has simply been modified by rotation during D3, related to the shear zone. However, we cannot rule out the possibility that the Akebono Rock F2 folds are unrelated to the regional Fm folds.

Based on aeromagnetic data, Nogi *et al.* (2013) proposed a regional tectonic model for the evolution of the LHC. This model involves subduction, subsequent collision and then a dextral strike-slip event that emplaces an allochthonous, granulite-grade block at Cape Hinode. The orientations of the shear proposed by Nogi *et al.* (2013) (ENE–WSW) and the shear here (WNW-ESE) would appear to be slightly different. Our study shows that, at Akebono Rock, a dextral shear, which is probably related to this late-stage regional dextral event, also emplaced a higher-grade metamorphosed unit. However, at Akebono Rock, the dextral movement is accompanied by a normal fault component. From this, we suggest that the allochthonous granulite at Cape Hinode may not necessarily have been translated any great distance horizontally, but may represent a deeper part of the crust below Cape Hinode itself.

The observed shear zone at Akebono Rock is probably not wide enough to correspond to a crustal-scale feature. We suggest that it could be a minor splay or a shear related to a much larger feature that remains hidden under the ice sheet. In this regard, we note that there is a narrow, elongated outcrop of undifferentiated rock that follows the northern edge of the Akebono Glacier (Fig. 2). This outcrop trends E-W, which is parallel to the shear zone at Akebono Rock. This raises the possibility that this outcrop could be the site of a major, regional-scale shear zone and bears further investigation.

Conclusions

Deformation episodes are recognized at Akebono Rock. The main foliation S1 was accompanied by ductile folds F1, which are mainly preserved in the eastern part. During D2 isoclinal to tight asymmetric folds, F2 formed, accompanied by an S2 foliation that varies in strength. Where S2 is well developed, garnets have pressure shadows and asymmetric tails. These tails contain biotite, which also replaces the margins of the garnets. The D3 episode is the formation of a shear zone, within which mylonites and L-tectonites developed. There is some evidence that other shear zones may have been active between D1 and D2, emplacing an amphibolite with large sigmoidal garnets, as discussed below.

The mylonite and L-tectonite within the D3 shear zone have asymmetric textures, including C/S fabrics and mica fish, which suggest shear movement is an oblique normal slip with right-lateral motion. The mylonite and L-tectonite developed under *P-T* conditions of 610–660°C and 4–5 kbar. Garnets in the mylonite garnet are partially replaced by secondary biotite and muscovite along cracks that formed as they were drawn out into lensoidal shapes by movement along with Riedel shears of the C/S structures. This hydrous replacement probably occurred during retrogressive uplift.

Our discovery of large sigmoidal garnet in an amphibolite adjacent to the shear zone is the first detailed report of such rotated phenocrysts in the LHC. The cores of such garnets are characterized by S-shaped inclusion trails, whilst the rims have Z-shaped inclusion trails. This change suggests two separate phases of growth, both under syntectonic conditions. It is possible that the cores formed during prograde metamorphism, which reached peak *P-T* conditions of ~8 kbar and 650–700°C. The rims way have formed during isothermal decompression during uplift and emplacement into a Grt-leucogranite at the margin of what became the D3 shear zone, reaching *P-T* conditions of ~6 kbar and 650–700°C. The Grt-amphibolites in most of Akebono Rock contain euhedral garnets and are estimated to have been metamorphosed at similar *P-T* conditions (6 kbar and 650–700°C).

Although the shear zone at Akebono Rock is not considered to be a regional-scale feature, its deformation history may be similar to that of other major shear zones along the LHC coast (Fig. 13), some of which are possible terrane boundaries. In this regard, the uplift of the sigmoidal garnet-bearing amphibolite, metamorphosed earlier and at a greater depth than the other rocks found at Akebono Rock, indicates that the emplacement of the granulite facies inlier at Cape Hinode may involve more vertical than horizontal movement.

Supplementary material

Four supplemental tables will be found at https://doi.org/10.1017/S0954102020000450

Acknowledgements

We would like to thank the members of the 58th Japan Antarctic Research Expedition and the crew of the

icebreaker *SHIRASE*. We acknowledge Y. Hiroi, Y. Osanai, T. Toyoshima, K. Shiraishi, M. Owada and T. Kawasaki for valuable discussions and field information. SB and PN thank J. Booth for his improvement of the English and various comments. Constructive comments from K. Das, K. Sajeev and an anonymous reviewer improved this manuscript and are gratefully acknowledged.

Author contributions

SB conceived the study, completed data collection, analysis and data interpretation and wrote the paper. TH and AK contributed to the fieldwork, analysis of the study and preparation of the paper. IK, YM, PN, NIS and D-OD contributed to field sampling, observations and preparation of the paper.

Financial support

This work was partly supported by the National Institute of Polar Research (General Collaboration Projects 25–17), the Research Organization of Information and Systems (ROIS-DS-JOINT 004RP2018) and the Japan Society for the Promotion of Science (JSPS) (15K05346 to SB, 17H02976 to TH and 18H01313 to AK).

Conflict of interest

The authors state that they have no conflicts of interest.

References

Baba, S., Horie, K., Hokada, T., Owada, M., Adachi, T. & Shiraishi, K. 2015. Multiple collisions in the East African-Antarctica Orogen: constraints from timing of metamorphism in the Filchnerfjella and Hochlinfjellet Terranes in Central Dronning Maud Land. *Journal of Geology*, **123**, 55–77.

Bhattacharya, A., Mohanty, L., Maji, A., Sen, S.K. & Raith, M. 1992. Non-ideal mixing in the phlogopite-annite boundary: constraints from experimental data on Mg-Fe partitioning and a reformulation of the biotite-garnet geothermometer. *Contributions to Mineralogy and Petrology*, **111**, 87–93.

Hiroi, Y., Shiraishi, K. & Motoyoshi, Y. 1991. Late Proterozoic paired metamorphic complexes in East Antarctica, with special reference to the tectonic significance of ultramafic rocks. *In* Thomson, M.R.A., *ed. Geological evolution of Antarctica*. Cambridge, UK: Cambridge University Press, 83–87.

Hiroi, Y., Shraishi, K. & Sasaki, K. 1986. *Explanatory text of geological map of Akebono Rock, Antarctica. Antarctic geological map series, sheet 16 Akebono Rock*. Tokyo: NIPR.

Hiroi, Y., Motoyoshi, Y., Ishikawa, N., Hokada, T. & Shiraishi, K. 2008 Origin of xenocrystic garnet and kyanite in clinopyroxene-hornblende-bearing adakitic meta-tonalites from Cape Hinode, Prince Olav Coast, East Antarctica. *In* Satish-Kumar, M., Motoyoshi, Y., Osanai, Y., Hiroi, Y., & Shiraishi, K., *eds.*, Geodynamic evolution of East Antarctica: a key to the east-west Gondwana connection. *Special Publication of the Geological Society of London*, No. 308, 333–350.

Hiroi, Y., Motoyoshi, Y., Satish-Kumar, M., Kagashima, S., Suda. Y. & Ishikawa, N. 2006. Granulites from Cape Hinode in the amphibolite-facies eastern part of Prince Olav Coast, East Antarctica: new evidence for allochthonous blocks in the Lützow-Holm Bay Complex. *Polar Geoscience*, **19**, 89–108.

Hodges, K. & Spear, F.S. 1982. Geothermometry, geobarometry and the Al_2SiO_5 triple point at Mt. Moosilauke, New Hampshire. *American Mineralogist*, **67**, 1118–1134.

Hoisch, T.D. 1990. Empirical calibration of six geobarometers for the mineral assemblage quartz + muscovite + biotite + plagioclase + garnet. *Contributions to Mineralogy and Petrology*, **104**, 225–234.

Holdaway, M.J. 2000. Application of new experimental and garnet Margules data to the garnet-biotite geothermometer. *American Mineralogist*, **85**, 881–892.

Holland, T. & Blundy, J. 1994. Non-ideal interactions in calcic amphiboles and their bearing on amphibole-plagioclase thermometry. *Contributions to Mineralogy and Petrology*, **116**, 433–447.

Hawthorne, F.C., Oberti, R., Harlow, G.E., Maresch, W.V., Martin, R.F., Schumacher, J.C. & Welch, M.D. 2012. Nomenclature of the amphibole supergroup. *American Mineralogist*, **97**, 2031–2048.

Ikeda, T. & Kawakami, T. 2004. Structural analysis of the Lützow-Holm Complex in Akarui Point, East Antarctica, and overview of the complex. *Polar Geoscience*, **17**, 22–34.

Ishikawa, M., Motoyoshi, Y., Fraser, G. L. & Kawasaki, T. 1994. Structural evolution of Rundvågshetta region, Lützow-Holm Bay, East Antarctica. *Proceedings of the NIPR Symposium on Antarctic Geosciences*, **7**, 69–89.

Jacobs, J. & Thomas, R.J. 2004. Himalayan-type indenter-escape tectonics model for the southern part of the late Neoproterozoic-early Paleozoic East African-Antarctic Orogen. *Geology*, **32**, 721–724.

Jacobs, J., Opås, B., Elburg, M.A., Läufer, A., Estrada, S., Ksienzyk, A.K., *et al*. 2017. Cryptic sub-ice geology revealed by a U-Pb zircon study of glacial till in Dronning Maud Land, East Antarctica. *Precambrian Research*, **294**, 1–14.

Kawakami, T. & Ikeda, T. 2004. Structural evolution of the Ongul Islands, Lützow-Holm Complex, East Antarctica. *Polar Geoscience*, **17**, 12–21.

Kohn, M.J. & Spear, F.S. 1990. Two new geobarometers for garnet amphibolites, with applications to southeast Vermont. *American Mineralogist*, **75**, 89–96.

Le Breton, N. & Thompson, A.B. 1988. Fluid-absent (dehydration) melting of biotite in metapelites in the early stages of crustal anatexis. *Contributions to Mineralogy and Petrology*, **99**, 226–237.

Locock, A.J. 2014. An Excel spreadsheet to classify chemical analyses of amphiboles following the IMA 2012 recommendations. *Computers and Geosciences*, **62**, 1–11.

Meert, J. 2003. A synopsis of events related to the assembly of east Gondwana. *Tectonophysics*, **362**, 1–40.

Motoyoshi, Y. & Ishikawa, M. 1997. Metamorphic and structural evolution on granulites from Rundvagshetta, Lützow-Holm Bay, East Antarctica. *In* Ricci, C.L., *ed. The Antarctic region: geological evolution and processes*. Siena: Terra Antarctica, 65–72.

Nakai, Y., Kano, T. & Yoshikura, S. 1980. *Explanatory text of geological map of Cape Ryûgû, Antarctica. Antarctic geological map series, sheet 15 Cape Ryûgû*. Tokyo: NIPR.

Nogi, Y., Jokat, W., Kitada, K. & Steinhage, D. 2013. Geological structures inferred from airborne geophysical surveys around Lützow-Holm Bay, East Antarctica. *Precambrian Research*, **234**, 279–287.

Osanai, Y., Nogi, Y., Baba, S., Nakano, N., Adachi, T., Hokada, T., *et al*. 2013. Geologic evolution of the Sør Rondane Mountains, East Antarctica: collision tectonics proposed based on metamorphic processes and magnetic anomalies. *Precambrian Research*, **234**, 8–29.

Passchier, C.W. & Trouw, R.A. 1996. *Microtectonics*. Berlin: Springer, 289 pp.

Powell, C.McA. & Vernon, R.H. 1979. Growth and rotation history of garnet porphyroblasts with inclusion spinels in a Karakoram schist. *Tectonophysics*, **54**, 25–43.

Robyr, M., Carlson, W.D., Passchier, C. & Vonlanthen, P. 2009. Microstructural, chemical and textural records during growth of snowball garnet. *Journal of Metamorphic Geology*, **27**, 423–437.

Shiraishi, K., Hokada, T., Fanning, C.M., Misawa, K. & Motoyoshi, Y. 2003. Timing of thermal evens in east Dronning Maud Land, East Antarctica. *Polar Geoscience*, **16**, 76–99.

Shiraishi, K., Dunkley, D.J., Hokada, T., Fanning, C.M., Kagami, H. & Hamamoto, T. 2008. Geochronological constraints on the late Proterozoic to Cambrian crustal evolution of East Dronning Maud Land, East Antarctica: a synthesis of SHRIMP U-Pb age and Nd model age data. *In* Satish-Kumar, M., Motoyoshi, Y., Osanai, Y., Hiroi Y. & Shiraishi, K., *eds.*, Geodynamic evolution of East Antarctica: a key to the east-west Gondwana connection. *Special Publication of the Geological Society of London*, No. 308, 21–67.

Shiraishi, K., Ellis, D.J., Hiroi, Y., Fanning, C.M., Motoyoshi, Y. & Nakai, Y. 1994. Cambrian orogenic belt in East Antarctica and Sri Lanka: implication for Gondwana assembly. *Journal of Geology*, **102**, 47–65.

Stern, R.J. 1994. Arc assembly and continental collision in the Neoproterozoic East Africa Orogen: implications for the consolidation of Gondwana. *Annual Review of Earth and Planetary Sciences*, **22**, 319–351.

Suda, Y., Kawano, Y., Yaxley, G., Korenaga, H. & Hiroi, Y. 2008. Magmatic evolution and tectonic setting of metabasites from Lützow-Holm Complex, East Antarctica. *In* Satish-Kumar, M., Motoyoshi, Y., Osanai, Y., Hiroi, Y. & Shiraishi, K., *eds.*, Geodynamic evolution of East Antarctica: a key to the east-west Gondwana connection. *Special Publication of the Geological Society of London*, No. 308, 211–233.

Takahashi, K., Tsunogae, T., Santoshi, M. & Takamura, Y. 2018. Paleoproterozoic (*c.* 1.8 Ga) arc magmatism in the Lützow-Holm Complex, East Antarctica: implications for crustal growth and terrane assembly in erstwhile Gondwana fragments. *Journal of Asian Earth Sciences*, **157**, 245–265.

Takamura, Y., Tsunogae, T., Santosh, M. & Tsutsumi, Y. 2018. Detrital zircon geochronology of the Lützow-Holm Complex, East Antarctica: implications for East Antarctica - Sri Lanka correlation. *Geoscience Frontiers*, **9**, 355–375

Talarico, F.M., Stump, E., Gootee, B.F., Foland, K.A., Palmerri, R., van Schmus, W.R., *et al*. 2007. First evidence of a 'Barrovian'-type metamorphic regime in the Ross orogen of the Byrd Glacier area, central Transantarctic Mountains. *Antarctic Science*, **19**, 451–470.

Tsunogae, T., Yang, Q.Y. & Santosh, M. 2015. Early Neoproterozoic arc magmatism in the Lützow-Holm Complex, East Antarctica: petrology, geochemistry, zircon U-Pb geochronology and Lu-Hf isotopes and tectonic implications. *Precambrian Research*, **266**, 467–489.

Whitney, D.L. & Evans, B. 2010. Abbreviations for names of rock-forming minerals. *American Mineralogist*, **95**, 185–187.

Wu, C.M. & Chen, B.H. 2006. Valid garnet-biotite (GB) geothermometry and garnet-aluminum silicate-plagioclase-quartz (GASP) geobarometry in metapelitic rocks. *Lithos*, **89**, 1–23.

Wu, C.M. & Zhao, G.C. 2007. The metapelitic garnet-biotite-muscovite-aluminosilicate-quartz (GBMAQ) geobarometer. *Lithos*, **97**, 365–372.

Yoshida, M. 1979. Tectonics and metamorphism of the region around Lutzow-Holmbukta, East Antarctica. *Memoirs of National Institute of Polar Research Special Issue*, **14**, 28–40.

Yoshimura, Y., Motoyoshi, Y. & Miyamoto, T. 2008. Sapphirine + quartz association in garnet: implication for ultrahigh-temperature metamorphism at Rundvågshetta, Lützow-Holm Complex, East Antarctica. *Special Publication of the Geological Society of London*, No. **308**, 377–390.